Republic of Iraq
Ministry of Higher Education and Scientific Research
Al-Nahrain University

Analytical –Computational Study of the Reflecting Telescope Parameters

A Thesis
Submitted to the College of Science in Partial Fulfillment of the Requirements for the Degree of Master of Science
in
Physics

NOUR MOHAMMED HASSAN YASEEN
B.Sc. Phys.2004

Muharram 1428 H.
December 2006A.D

بسم الله الرحمن الرحيم

إِنَّ فِي خَلْقِ السَّمَاوَاتِ وَالأَرْضِ وَاخْتِلاَفِ اللَّيْلِ وَالنَّهَارِ لآيَاتٍ لِّأُوْلِي الألْبَابِ

الَّذِينَ يَذْكُرُونَ اللّهَ قِيَامًا وَقُعُودًا وَعَلَىَ جُنُوبِهِمْ

وَيَتَفَكَّرُونَ فِي خَلْقِ السَّمَاوَاتِ وَالأَرْضِ رَبَّنَا مَا خَلَقْتَ هَذا بَاطِلاً سُبْحَانَكَ فَقِنَا

عَذَابَ النَّارِ

صدق الله العظيم

سورة آل عمران ﴿١٩٠-١٩١﴾

الإهداء

أليك يا من لاتمر لحظة ألا وأحبك أكثر وأفتقدك أكثر وأكثر وأدرك أنك أكبر وأكبر من الحياة والموت معاً .ربما رحلت عني ولكنك هنا أبداً في قلبي وروحي وفي صحوي وأحلامي . . .

أخي مظهر

أليك يا من أنت لي قيمة أعلى ومعناً أسمى . . .

أ .د .صباح محمود جمعة

شكر و تقدير

في البدء . . يا كل من أحمل لهم كل ألتقدير و أدين لهم بكل ألشكر لنصائحهم ودعمهم وتشجيعهم المتواصل لي أستميحكم عذراً لان ابلغ كلمات الشكر وأجزلها معنىً لاتفيكم ولو قليلاً من حقكم علي . ولكن عذري الوحيد ان الكلمات هي لغة تواصلنا الوحيدة التي تتجاوزها تطورا بقرون لغة المعاني والمشاعر و منها عميق الاحترام الذي اكنّه لحضراتكم

جزيل شكري اليكم . .

. . أستاذي الفاضل رمز كل القيم الانسانية ، و مثلاً أتشرف السير على خطاه، أ . د . صباح لكل الجهود الذي بذلتها في مشروع البحث، رحمك الله تعالى فقد كنت وستظل نعم الأستاذ و الأب الموجه والمعلم .

. . . استاذي القدير د . أحمد لحثيث الجهود والأشراف العلمي المتواصل والدعم الذي تفضلتم به حضرتكم كأستاذ مشرف على أطروحتي وكرئيس لقسم الفيزياء .

والشكر موصول لكل منتسبي قسم الفيزياء و زملائي الأعزاء لكل مساعداتهم القيمة .

ولايسعني إلا ان أتقدم بعميق التقدير وكثير الشكر الى عميد كلية العلوم الدكتور ليث عبد العزيز العاني .

ملاذي الأمن دوماً أمي الحبيبة، أختي العزيزة سهير ، وبقية افراد أسرتي .

وأخيراً في سياق الترتيب فحسب والأول دائماً بالنسبة لي أستاذي وزوجي العزيز أستاذ إبراهيم لمجهودات اكبر من ان تسعفها الكلمات .

نور محمد

كانون الاول 2006

Certificate

I certify that this thesis, entitled: ***Analytical-Computational Study of the Reflecting Telescope Parameters***" prepared by *NOUR MUHAMMED HASSAN YASSIN* was under my supervision at AL-Nahrain University, College of Science in partial fulfillment of the requirements for the degree of Master of Science in Physics.

Signature
Supervisor : Dr. Ahmad Kamal Ahmad
Date :   / 12 / 2006

In view of the recommendation, I present this thesis for debate by the examining committee

Signature
Head of Department: Dr. Ahmad Kamal Ahmad
Date :   / 12 / 2006

Examining Committee Certificate

We certify that we have read this thesis, entitled ***"Analytical- Computational Study of the Reflecting Telescope Parameters",*** and as an examining committee, examined the student **NOUR MOHAMMED HASSAN YASEEN** on its contents, and that in our opinion it is adequate for the partial fulfillment of the requirements for the degree of Master of Science in Physics.

Signature:
Name: Ayad A. Al-Ani (Chairman)
Title: Assistant Professor
Date: / 2 / 2007

Signature:
Name: Mohammed Ahmed Salih (Member)
Title: Senior Scientific Researcher
Date: / 2 / 2007

Signature:
Name: Dr. Ali H. Al-Hamdani (Member)
Title: Assistant Professor
Date: / 2 / 2007

Signature:
Name: Dr. Ahmad Kamal Ahmad (Member)
Title: Assistant Professor
Date: / 2 / 2007

Approved to the University Committee of Postgraduate Studies.

Signature:
Dean of College of Science: Dr. Laith Abdulaziz Al-Ani
Title: (Assistant Professor)
Date: / 2 / 2007

Abstract

In this work, a program of ray tracing program has been constructed. This program includes ray tracing for:

1. Skew ray tracing for spherical surfaces;
2. Skew ray tracing for Cartesian or quadric surfaces of revolution (conic surfaces).

A study for the effect of asphericity factor (ε) on the reflecting telescope parameters under investigation of this thesis has been accomplished by using the ray tracing code. These parameters are the Δ-values (values for surface departure from the spherical), ray aberrations both the transverse (TA) and the longitudinal (LA), and the angle the incident ray makes with the surface normal vector.

This study was useful to design a two-mirror reflecting telescope; it gave a suitable scope of understanding the problem sides, and provided a vision to minimize, directly, aberrations and consequently improving the optical system performance.

Accomplishing this study demanded considering the bundle of incoming light rays as completely parallel to the optical axis; therefore, the design of the optical system is corrected for spherical aberrations only.

The ray tracing code has been employed to exhibit the performance of the reflecting surfaces (mirrors) when the asphericity factor (ε) is varying. Rays aberrations (transverse and longitudinal) aberrations have been considered as a measure to exhibit the performance of any conic reflecting surface (mirror) versus ε.

Aberrations reduction has been achieved through modifying, first, the secondary mirror radius of curvature and, second, the aspherisity factor (ε) by using the principle of the Extreme-Value Theorem.

The design of the telescope, achieved upon this study, is a two-mirror system of 2.5m focal length corrected for spherical aberrations; the primary mirror is paraboloid of 1m aperture and 5m radius of curvature and the secondary is hyperboloid of asphericity factor ε = - 0.21.

The considered light wavelength in the calculations concerning the telescope is 550nm because it is in the middle of visible spectrum of light.

Contents

Abstract		*I*
Contents		*II*
Chapter 1:	*Introduction*	
	1.1 Introduction	*1*
	1.2Reflecting Telescope Configurations	*3*
	1.3 Advantages of Reflection Telescope	*5*
	1.4 Telescope Three Powers	*6*
	1.4.1 Magnification Power	*6*
	1.4.2 Resolving Power	*6*
	1.4.3 Light-Gathering Power	*8*
	1.5 Ideal Image Formation	*9*
	1.6 Aberrations	*10*
	1.7 Historical Aspect	*13*
	1.8 Recent advances in Astronomical Telescopes Design	*14*
	1.8.1 Fabrication of Large Astronomical Mirrors	*15*
	1.8.2 Active Optics Control Systems	*17*
	1.8.3 Primary Mirror Segmentation	*18*
	1.8.4 Progress in Polishing of Large Mirrors	*21*
	1.8.5 Progress in Optical Testing of Large Mirrors	*23*
	1.9 The Aim of Thesis	*24*
Chapter 2:	*2.1Ray Tracing*	*25*
	2.2 Skew Ray Tracing through Spherical Surfaces	*26*
	2.3 Ray Tracing through Quadric of Revolution	*31*
	2.4 Computing Transverse (TA) and Longitudinal (LA) Aberrations	*35*
Chapter 3:	*Results and Discussion*	*36*
	3.1 Discussing Surfaces' Shapes	*37*
	3.2 Discussing the Telescope's Parameters	*42*
	3.3 Conclusions	*55*
Chapter 4:	*The Basic Design of Reflecting Telescope*	
	4.1 Design Steps	*57*
	4.2 The Extreme-Value Theorem	*58*
	4.3 Optimum Secondary Mirror Radius Determination	*59*
	4.4 Telescope Characteristics	*61*
	4.5 The Telescope Features	*62*
	4.6 Conclusions	*63*
	4.7 Future Work	*63*
Appendix		*64*
References		*69*

Chapter 1

1.1 Introduction

The telescope invention in the 17th century opened up a window that completely revolutionized the face of astronomy. This instrument allowed an observer to study the precise configuration of celestial bodies and piece together theories about the structure of the universe in a way previously impossible [1].

Ground- and space-based optical astronomy has developed rapidly over the last decade. A series of sensational discoveries has been made in stellar and extragalactic astronomy: proto-planetary disks and even planets have been detected around nearby stars; compelling evidence has been found of the presence of a massive black hole in the central part of many galaxies, including our own; the ages of distant galaxies and quasars have been estimated. These astonishing achievements in optical astronomy are mainly associated with the successful completion of several large optical telescope projects. With a new generation of ground-based telescopes having a primary mirror diameter of 8-10 meters, the total collecting area of optical telescopes has grown exponentially and now exceeds 1000 square meters. The creation of these large optical ground-based telescopes with even higher image quality than their predecessors has become possible due to[2]:

* progress in computer control techniques;
* technological advances in manufacturing of large astronomical mirrors;
* successful employment of *adaptive optics* (AO) for the correction of image distortion introduced by turbulence in the Earth's atmosphere.

Together with the increasing aperture size of this new generation of telescopes, the accuracy of their operation and guiding system has become exceedingly high. This is partly due to a substantial mass reduction for the primary mirror and the telescope as a whole. By actively supporting the light, thin primary mirrors, their shape can be maintained under changing orientation (pointing) of the telescopes.

Image stabilization and correction of atmospheric distortion are achieved using AO systems, which are capable of correcting for the effect of the Earth's atmosphere. Within such corrected fields, the image quality is limited only by telescope optics, which thanks to current technology can be made diffraction-limited. Taking these facts into account, it is a common belief that the creation of an *Extremely Large Telescope* (ELT) with 25-100 m aperture is realistic nowadays. Whether such a complex project succeeds, primarily depends on the correct choice of the telescope system configuration.

The focal ratio and asphericity of the primary are the main factors influencing the system configuration. Since minimization of the total number of optical components and system complexity is of great importance, integration of an AO system into the telescope is one of the key considerations for the ELT concept. The optical system for an ELT should have [2]:

- A fast primary mirror;
- An AO system as an integrated part of the telescope design;
- Diffraction-limited image quality over $1'$-$2'$ field of view.

These basic requirements have been considered and fulfilled for the Euro50 ELT with an aperture of 50 m; where Euro50 is the most modern telescope project under achievement [2].

Most optical surfaces are spherical because a spherical surface is the easiest to produce [3]. The difficulty of figuring aspheric optics by traditional means is approximately in proportion to the slope of the aspheric departure. As surfaces depart more and more from a spherical shape, increasingly smaller tools are required to obtain a reasonably good fit between the tool and the optical surface [4]. However, non-spherical are necessary for some purposes, especially when they appear as the solution of particular optical problems, where one of these surfaces, ellipse, is the one that verifies Fermat's principle which states that the optical path length of each ray will be identical [3].

On the light of this introduction, it is believed that investigating the effect of the asphericity factor is of great deal of importance since the aspherical (non-spherical) surfaces provide a solution to the problem of image forming systems; and reflecting telescopes are, of course, type of these systems.

1.2 Reflecting Telescopes Configurations

Reflecting telescope are mainly come in four configurations [5]:

1. Herschel Telescopes :

These telescopes consist of one mirror (the primary only) aligned in such a manner that allows the gathered light to pass out the telescope housing tube, in order to enable the observer to see the formed image, by flipping the mirror slightly from the right angle the mirror makes with the optical axis. The essence of this design (arrangement) is to make the full use of the whole aperture(whole surface area of the mirror), i.e., without obstruction as shown in figure 1.1. The existence of another mirror (secondary) before the primary, the secondary, will prevent (obstruct) some of the light coming from the left to reach the primary mirror. And this is exactly the case of the next types. But the advantage of the next types over the Herschel are the control of aberrations with more symmetrical mirror arrangements is easier.

2. Newtonian Telescopes:

Besides the primary mirror there is a small plane mirror near to its focus. The function of the plane mirror is to guide the light outside the housing tube of the telescope to enable the observer to see the formed image as shown in figure 1.2.

3. Gregorian Telescopes:

These telescopes consist of two mirrors. The second one (secondary) is also concave but of much smaller aperture lest it should obstruct large amount of light the primary should gather. So, the secondary main function is to direct the light reflected from the primary to be focused behind the primary mirror through a cavity at the center of the latter as shown in the figure 1.3.

4. Cassegrian Telescopes:

These telescopes do not differ from the Gregorian accept that secondary mirror is convex rather than being concave as shown in figure1.4.

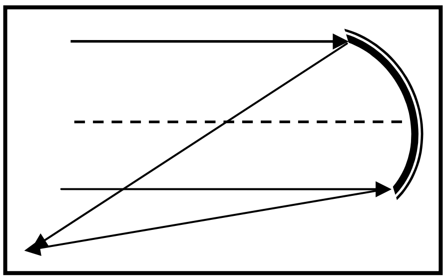

Figure1.1 Herschel Telescope [5].

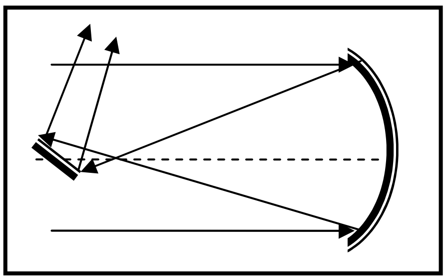

Figure1.2 Newtonian Telescope [5].

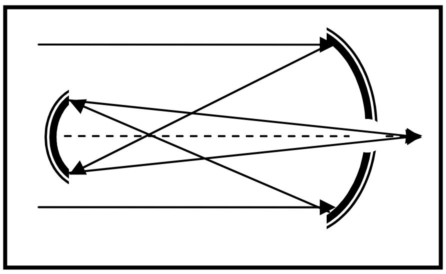

Figure1.3 Gregorian Telescope [5].

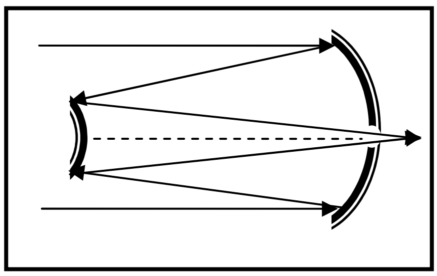

Figure1.4 Cassegrian Telescope [5].

1.3 Advantages of Reflecting Telescope

There are several advantages for these telescopes over the refraction telescopes because of using mirrors rather than lenses. These advantages are [5, and 6]:

1. Reflecting telescopes are free of chromatic aberration.
2. It is easier to increase the aperture of a mirror than increasing the aperture of a lens. This because as it's very well know that lens has thickness; so, if the increase in the mirror diameter weight is in hundreds of kilograms; the similar increase in the diameter of lens in meters leads to the increase in the lens weight in tons of kilograms. And this in turn would make any attempt for porting or moving it very hard; besides it is approximately impossible to manufacture such lenses with high lens performance (image quality), unless they would be broken under their extensive weight, due to the problems arise from bubbles formation and cracks during manufacturing.
3. Reflecting telescopes form images brighter than that refraction telescopes form.
4. as it's known, lenses are suitable for gathering light through refraction for a very narrow band width of the spectrum(visible region 400-700 nm and IR light); whilst mirror are suitable for gathering light through reflection for very vast range of wavelength; from the X-rays up to the radio waves; and that's why reflecting telescopes enables user to observer and see different pictures of the celestial bodies to be observed.

1.4 Telescope Three Powers

There are three features (powers) of a telescope that enable them to extend the power of our vision: a telescope's superior light-gathering ability(light-gathering power) enables us to see faint objects, a telescope's superior resolving power enables us to see even the tiniest of details, and the magnification power enables us to enlarge tiny images. Magnification is the least important power of a telescope. Specialists know that the light-gathering power and resolving power are the most important. These two abilities depend critically on the objective, so they make sure the optics of the objective are excellent [7].

1.4.1 Magnification Power

It is the ability to make the image bigger. Since the amount of detail we can see is limited by the seeing conditions and the resolving power, very high magnification does not necessarily show us more detail. Magnification can be changed by simply switching eyepieces in the telescope [5]. The magnification of a telescope is the ratio of the focal length of the objective lens or mirror F_O divided by the focal length of the eyepiece F_E [5]:

$$M = F_O / F_E \tag{1.1}$$

1.4.2 Resolving Power

It is a measure of how sharp and well-defined an image the telescope can produce or the telescope's ability to resolve fine details. This ability depends on a combination of both its aperture and telescope optics. Whenever light is focused into an image, a blurred fringe surrounds the image. Because this diffraction fringe surrounds every point of light in the image, we can never see any detail smaller than the fringe. There is nothing we can do to eliminate diffraction fringes; they are produced by the wave nature of light. If we use a large diameter telescope, however, the fringes are smaller and we can see smaller details. Thus; the larger the is telescope, the better its Resolving Power [5].

Suppose a telescope is used to observe two stars close together. In the focal plane the best possible images instead of being points are two Airy diffraction patterns, each being a circular spot surrounded by alternate bright and dark rings. Rayleigh suggested that the angular (separation) resolution of a telescope should be defined as the angle between two stars when the maximum of the diffraction pattern of one falls exactly on the first minimum of the other. That's to say [5]:

$$\text{Angular resolution power} = \alpha_o = 1.22\frac{\lambda}{D} \tag{1.2}$$

where λ is the wavelength and D is the objective diameter(aperture).

If the angular separation (resolution power) of the two stars is α_o then the centers of the two diffraction patterns are separated by a distance $\alpha_o f$ in the focal plane. Hence according to equation(1.2), the linear separation between the centers of the diffraction patterns is expressed as:

$$\text{Linear separation} = 1.22\frac{\lambda}{D}.f \tag{1.3}$$

So, this expression enables scaling the system up and down simply by changing f but unfortunately without altering the relative size of the diffraction patterns and their separation [5].

According to [8], equation (1.3) is not very accurate, because it depends on the focal length to the diameter ratio (for most telescopes, the radius of the primary mirror is small in comparison to the focal length), which means that the primary mirror is relatively "flat" and that's why it is just an approximation. The same reference introduced another expression derived for exact linear separation as:

$$\text{Linear separation} = 1.22\ \frac{\lambda}{n.\sin(U)} \tag{1.4}$$

where n is the surface refractive index and *U* is the extremely marginal ray convergence angle. Reference [8] predicts that in the case of paraboloid, primary mirror the focal length is nearly equal to the mirror diameter, a very small Airy disc which can be attained, of course, means exceptional resolution. In fact, it attains a resolution better than any conventional telescope. And, since it was shown that resolution is determined by the angle *U*, and not by the ratio of focal length to the diameter, as is implied by the "approximation" equation (1.2), this configuration (deep-dish mirrors) can be used for mirrors of any size, even very small sizes, while still remaining exceptional resolution [8].

1.4.3 Light-Gathering Power

Refers to the ability of a telescope to gather (collect) light. Light-gathering power is probably its most important feature. Stars are faint. Even the brightest stars appear 25 billion times fainter than the Sun, and most interesting celestial objects are much fainter than that [9], so we need a telescope that can gather large amounts of light to produce a bright image.

Catching light in a telescope is like catching rain in a bucket, the bigger the bucket, the more rain it catches. A large diameter telescope (*large aperture*) gathers more light and has a brighter image than does a smaller telescope of the same focal length. Light-gathering power is proportional to the area of the telescope objective. A lens or mirror with a large area gathers a large amount of light. Because the area of a circular lens or mirror of diameter *D* is $pi(D/2)^2$, we can compare the areas of two telescopes, and therefore their relative light-gathering powers, by comparing the square of their diameters. That is, the ratio of the light-gathering power (LGP) of the two telescopes A and B is equal to the ratio of their diameters squared [10]:

$$LGP_A / LGP_B = (D_A/D_B)^2 \tag{1.5}$$

That’s why astronomers use big telescopes and why they refer to telescopes by diameter. In optical telescopes the increase of light-gathering power which is given bigger objectives brings with it an increase of resolving power. The world’s biggest telescopes have been made big for light-gathering power rather than high resolution, and in practice the theoretical diffraction limits of resolution is not attained because of bad “seeing” through the atmosphere. This is why the best earth-based photographs of the moon and the planets come from observatories famous for good seeing rather than for big telescopes [5].

1.5 Ideal Image Formation

Before introducing aberrations it is important to define the formation of ideal image for a comprehensive understanding to aberrations.

The rays from each point object intersect the Gaussian image point and spherical wave converges to the latter so that the disturbances, which have passed through different zones of the aperture, arrive exactly in phase (perfect imagery definition) [11]. This means, in ideal or perfect, optical system must surely be one in which every point in an object space corresponds precisely to a point in an image space, being connected to it by rays passing through all points of all optical system (perfect image forming system definition)[5]. So, the optical path from any object point to its image point is therefore the same along all rays [5].

1.6 Aberrations

Aberrations are the problem of all image–forming systems. They, in general, are defined as the departure from the Gaussian (paraxial) image formation [5]. Sometimes, they are called image defects or imperfections, because their presence causes deformation or complete damage to the image features. Therefore, optical systems possessing aberrations must be redesigned to get systems with an acceptable performance. The defect of the image may be said to be caused by the failure of the rays from a point source to unite at the Gaussian image point (rays aberration), or by the failure of the emergent wavefront to be a sphere converging on this point and the consequent failure of the disturbance to arrive exactly in phase (wavefront aberrations)[11].

The two concepts of rays and waves are the two basic ways to characterize aberrations. Rays aberrations come in three types [12]:

1. Longitudinal the rays intersect the optical axis);
2. Transverse or lateral (whereas the rays intersect the Gaussian Image plane);
3. Angular (directly related to the transverse);

Figure (1.5) shows these aberrations as LA, TA, and a, respectively. The wavefront is the actual light wave, where the ray is its normal vector reference and the reference sphere is the one that is responsible for free aberration.

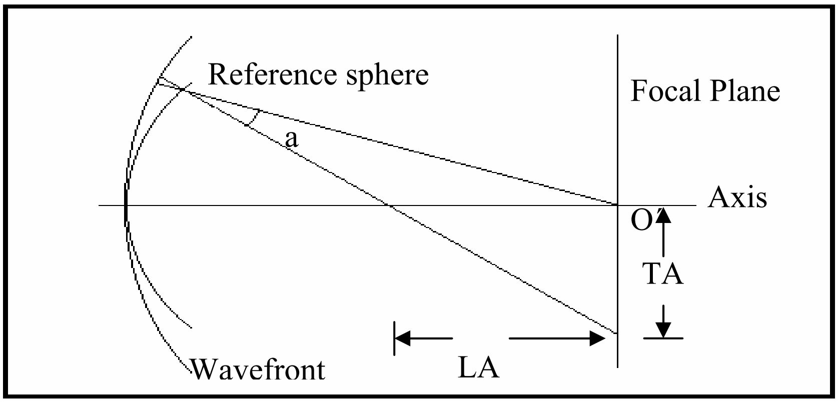

Figure (1.5) Longitudinal aberration (LA), transverse aberration (TA), and angular aberration of the meridianal ray (a) [12].

The position of an object relative to the optical axis produces two divisions of aberrations, the on–axis and off–axis. The on–axis one is the one that is produced by objects on the axis of revolution (optical axis), and its only effect is " *spherical aberration*", representing the different actions of the axial and peripheral rays [13]. But this is not the general case. The off–axis is the general one, which produces the five kinds of monochromatic aberrations. The aberrations, which occur when the laws of refraction and reflection are applied to mathematically correct surfaces and which are not a consequence of material inhomogenity or fabrication errors, are as follows[13]:

1. <u>Spherical aberration:</u>

It is defined as the longitudinal variation of the focus with aperture [14]. This phenomenon occurs wherein rays passing through different zones of a surface come to different foci. It is like chromatic aberration both have longitudinal (axial) and transverse (lateral) variety [15];

2. <u>Coma:</u>

Coma is the result of oblique rays, It is defined as the variation of magnification, i.e., image size with aperture. Thus, when a bundle of oblique rays are incident on a lens, the rays passing through the edge portions of the lens are imaged at a different height than those passing through the center portion [15];

3. <u>Astigmatism :</u>

It is another off-axis aberration. It is caused by the fact that the lens has different powers in the sagittal and the tangential sections;

4. <u>Field curvature or Petzval</u>:

It is another off-axis aberration, closely related to astigmatism (and it nearly accompanies astigmatism). But this type does not cause any image blur as the previous three do [14]. It is usually indicated as the departure of the image from a flat image plane [16];

5.Distortion:

It is the counterpart of field curvature. Like the later, distortion refers to a side way (radial) displacement of the image points, either toward or a way from the optical axis, in other word, it refers to a change of magnification [16].

These are monochromatic aberrations and were originally defined by Seidel in 1856. The importance of this classification declines as the system is more highly corrected. The higher order aberrations are not easily visualized as the primaries, and their particular forms differ according to which of several systems is used for expressing them. In actual image–forming system, deformed image is not because one of these aberrations but is, mostly, of a mixture of them [12].

1.7 Historical Aspect

In attempting to present, in an orderly way, the knowledge acquired over a period of several centuries in such a vast field; It is almost impossible, in this thesis, to follow the development of telescope designs due to the large variety of types, applications, and techniques. So, it is found that giving a brief historical aspect, in this section, and recent advances in telescopes in the coming sections would cover the story of literature survey.

According to [17] in the 17th century, 1608 a Holland(meant Dutch) spectacle maker, Hans Lippershy, is said to have been holding two lenses and he happened to align them before his eyes with the steeple of a near by church he was astonished to find the weather cock to appear nearer. Then when he fitted the two lenses in a tube to maintain their spacing, he had constructed the first telescope. Galilo Galilie in Venice heard about the new telescope in June 1609, and immediately began to make telescope of his own. His first had magnification of 3X, but his instruments were rapidly improved until he achieved magnification of about 32X.

Developers of early telescope soon recognized spherical aberration as a reason for defective images and a considerable effort was spent to overcome this fault. And when the telescope magnification approached 50X the developers noticed the appearance of chromatic aberration. In 1666, Isaac Newton discovered that refractive by given lens depended upon the color and he correctly concluded that the most significant defect of the then current telescopes was what we know as "chromatic aberration". He hastily concluded that all glasses had the same relation between refraction and color, so he turned to reflectors to solve the color problem [17].

1.8Recent Advances in Astronomical Telescope Design

A major rationale for building a new generation of telescopes with larger apertures is to increase the *angular resolution* and the *signal-to-noise ratio* so that telescopes become more sensitive to dim or distant objects. The signal-to-noise ratio depends on the physical parameters of a telescope and the sky background. For a dim point source with brightness not exceeding the sky background this ratio is [1]† (coming references denoted by [#]† belongs to [2] and pointed out in the references by the same manner also.):

$$\frac{S}{N} = k_m \frac{D\tau^{1/2}}{\rho\varepsilon^{1/2}}$$

where k_m is a coefficient depending on source brightness, D is the telescope aperture, τ is the effective throughput of the telescope to the focal plane (taking into account atmosphere, telescope optics and quantum efficiency of the detector), ρ is the angular size of the image, and ε is the effective emissivity of the sky background. Thanks to advances in detector quantum efficiency and readout noise, the effective throughput is approaching its maximum value. The sky background has minimum emissivity at some of the best astronomical sites [2]†. Therefore one may increase telescope sensitivity only by enlarging the telescope aperture D and delivering images of smaller diameters [3]†. As shown in section 1.8.1, primary mirrors with larger diameters can be constructed due to improved fabrication and optical testing methods. Point source images with diameters comparable to the Airy disk have been achieved by means of *active*[4]† and *adaptive optics* systems [5-7]†.

The use of thin and fast segmented primary mirrors makes it possible for telescopes to be more compact, significantly reducing their total mass, and thereby leading to more cost-effective solutions. Telescope cost is related to aperture size via the well-known empirical expression [8]† :

$$L_T = k_T D^{2.6}.$$

For the new generation of telescopes, the proportionality coefficient k_T has been reduced by a factor of three [8]†.

At present, it seems feasible to construct an ELT with an aperture of 25-100 m [9-12]†. Both cost and practical considerations influence the optical design of ELTs. The general requirements that an optical design should satisfy are identified in the following sections.

1.8.1 Fabrication of Large Astronomical Mirrors

The most distinctive feature of the new generation of telescopes is a *lightweighted primary mirror* of 8-10 m diameter [13-20]†. This feature brings down the cost and increases the resonance frequency of the telescope structure. Reduction in the mirror mass is accomplished by the use of thin glass blanks or blanks with a *honeycomb structure* on the backside.

Progress in technology of *thin meniscus mirror* blank fabrication has enabled designers to reduce the mass of the mirrors, for which the *aspect ratios* (diameter/thickness) have been increased to 40, whereas for mirrors in the previous generation of telescopes, the aspect ratios did not exceed 8. Mass reduction plays a key role in successful fabrication of large monolithic mirror blanks.

At the present time, there are several well-established methods for fabrication of large, light-weighted astronomical mirror blanks. One method consists of assembling the mirror from a set of hexagonal fused silica plates, followed by sealing in the furnace, grinding the resultant blank and sagging it to a required radius on a sagging mould under secondary heating [21]†. The advantage of such a method is predictability of the fabrication process and its scalability also for even larger mirror blanks. At the moment, the largest mirror fabricated according to this method is the 8.3-m primary mirror with a 0.2-m thickness and 23-ton mass for the Subaru National Japanese Telescope [22]†.

The second fabrication method for large, lightweighted mirrors is based on a spin-casting process using a special glass ceramic material, Zerodur, with zero coefficient of thermal expansion. The mirror blank is cast into a form in the furnace rotating with constant velocity, thus achieving a parabolic shape with a required radius of curvature. For primary mirrors of 8.2-m diameter with a thickness of 0.175 m and a mass of 23 tons have been successfully obtained by applying this method for the Very Large Telescope (VLT) [23]†.

If the casting is made into a form with a bottom having a regular honeycomb structure, then the resulting mirror blank will get a negative (hollow) honeycomb structure on its back side. This method was pioneered by Roger Angel [24]†. The honeycomb structure allows a reduction of the mirror mass, while preserving the mirror bending stiffness. For this process, inexpensive borosilicate glass with low coefficient of thermal expansion is used, since it can be processed at a lower temperature than zero-expansion glass-ceramics. Of two blanks of equal diameter, the one with honeycomb structure can be made two times lighter and almost ten times more rigid than the other one with a thin meniscus shape. The currently largest monolithic mirror of 8.4m diameter and a mass of 16 tons has been made using the honeycomb method for the Large Binocular Telescope (LBT) [16]†.

1.8.2 Active Optics Control Systems

The shape of giant, thin, and, hence, quite flexible mirrors is maintained by means of an *active support system*, which can compensate for slowly varying deformations of the mirror shape with frequency up to 0.1Hz [25–27][†]. Active support systems are preferable for mirrors with diameter larger than 2.5m. Smaller mirrors typically have enough rigidity to sustain their own weight and maintain their shape, in which case the use of passive support systems is more appropriate. Active support systems become mandatory for large monolithic mirrors with diameters exceeding 4m. Such systems have hundreds of support points with a spacing on the order of $D/10$, where D is the mirror diameter.

The active support system is part of the *active optics* system, which contains also an optical part monitoring the shapes and displacements of the mirrors. The main function of the active optics system is to keep the required mirror shape through compensation of slow-varying deformations. The ultimate goal is to improve the quality of the telescope image. Correction of mirror shapes and relative positions is carried out using prescribed tables taking into account gradual changes in temperature and gravity during telescope operation. Edge sensors are used to detect relative displacements of mirror segments. Detection of residual errors in shape and displacement is accomplished in a closed loop with the use of an *image analyser*. Together with the temperature, wind and edge sensors the image analyser gives complete information on slowly varying sources of optical image degradation.

The principal component of the image analyser is a wavefront sensor. Usually it is a Shack-Hartmann wavefront sensor working with *natural guide stars* (NGS) in the telescope field of view and measuring local slopes of the wavefront in each *sub-aperture* [28,29][†]. Wavefront measurements from several NGSs permit estimation of additional detailed anomalous changes in temperature and gravity perturbing the shape of the mirrors and their positions in the telescope.

Together with corrections prescribed in a table for varying mirror deformations, the active support system is capable of compensating for up to some 20 microns (RMS) of that *global figuring* error caused by inaccuracy in the fabrication process. Assuming the active support system is functional, certain manufacturing tolerances for the global figuring error, e.g. astigmatism and spherical aberration, can be relaxed for large active mirrors. Further improvements of the active control system may allow varying the radius of curvature of a mirror, as well as its asphericity.

For a segmented mirror, the active optical system can also be applied to position the segments of the primary mirror if the upper spatial frequency of the wavefront sensor is high enough to resolve the segment tilts. The operation of such a system was successfully demonstrated on the two large optical telescopes Keck I and II, each having a 10-m primary mirror consisting of 36 hexagonal segments that form a single hyperbolic surface after proper positioning [14,15]†. A similar system will be used for the Gran Telescopio Canarias (GTC), which also has a 10-m segmented hyperbolic primary mirror [17, 30]†.

1.8.3 Primary Mirror Segmentation

Segmentation is an effective way to obtain a lightweighted primary mirror for large aperture optical telescopes. Therefore, mirrors with diameters 10m or larger are composed of small (1-2m) hexagonal segments. This also makes mirror handling and transportation manageable. The main optical problem associated with segmentation is to eliminate wavefront errors caused by inaccuracy in positioning of the segments. The technical challenge in maintaining the correct shape of a large segmented mirror is greater than for a large monolithic mirror of the same size. Hence, a majority of large optical telescopes in the 8 m class are built with thin monolithic primary mirrors [13, 16, 19, 20][†].

Segmentation of the primary mirror is an efficient way to extend the mirror size without extrapolating the corresponding process for mirror fabrication. Consequently, future giant telescopes will have fast segmented primary mirrors. The upper diameter limit of a mirror composed of small passive segments is defined by the complexity of their positioning system and the feasibility of rapid mass production of the segments.

To reduce the number of segments one wishes to use segments that are as large as possible. Unfortunately, large segments are difficult to transport and are thicker and thereby heavier than small segments. It has been shown that employment of active segments with diameters larger than 4m is not attractive [12][†]. At present, the concept of a segmented primary mirror with 1-2 m passive segments is considered most realistic.

For instance, in the daring Overwhelmingly Large Telescope project (OWL) [12][†], the spherical 100-m primary mirror is composed of 2000 passive identical 2-m segments. For the California ELT project (CELT), it has been proposed to make the 30m hyperbolic primary mirror out of 1098 passive 1m off-axis segments [9][†].

A more extreme example of a telescope having a segmented primary mirror is a "telescope" with a non-filled aperture. Such a telescope may be regarded as consisting of many separate small telescopes distributed in a certain pattern to cover the aperture [31, 32][†]. A special optical system should provide both angular combination and phasing of the light beams from the individual telescopes into a common focus. Notably, the first telescope of this type built was the Multiple Mirror Telescope (MMT) [33]†. A similar project, the National New Technology Telescope (NNTT), was proposed but not realized [34]†. Also the LBT, currently under construction, belongs to this group [16]†.

The main advantage of a non-filled aperture telescope is its compact construction, as the telescope length can be much smaller than the diameter of the working aperture (defined as the distance between the most remote small telescopes). The size of the working aperture exceeds the size of the combined collecting telescopes, resulting in higher angular resolution for some spatial orientations. The optical phasing system combines all beams in the common focus by means of auxiliary mirrors. This implies 5–7 extra reflections on the way to the final focus.

High-reflectance coatings for astronomical mirrors have been under development for many years. New methods may reduce light losses in multi-mirror optical systems for ELTs. Technology studies of protective silver coatings carried out at the Optikzentrum in Bochum, Germany, show very promising results [35]†. In the near future, one may expect an efficient technology for producing robust, highly reflective coatings on large (primary) mirrors resulting in reflection coefficients above 0.95 [36]†. Another study has been carried out in connection with the Gemini project, which involves the construction of two large telescopes with 8.2 m primary mirrors [20]†. Consequent reductions in light loss may lead to more extensive usage of multimirror optical systems, in particular four-mirror systems for ELTs with total optical throughput about 80% or higher.

1.8.4 Progress in Polishing of Large Mirrors

New methods for optical fabrication provide high-quality, fast mirrors of large diameters as required in compact optical systems for ELTs [37]†. The main difficulty in achieving steep aspherical surfaces is not related to the amount of material to be removed (proportional to the deviation of the surface from the corresponding *best-fit sphere*), but to the removal at different rates over neighbouring areas. Therefore the maximum slope difference between the aspheric surface and the best-fit sphere defines the effort needed for polishing.

Referring to Dierickx [21]†, for a conic surface, a polishing difficulty criterion δ_c can be defined as:

$$\delta_c = \frac{8(f/D)^3}{|b|}$$

where f is the focal length, D is the diameter of the optical surface and b is the deformation constant. The value δ_c is inversely proportional to the slope difference between the conic surface and the corresponding best-fit sphere. The smaller the value of δ_c , the more difficult is the aspherization. Small focal ratios (f/D) present severe problems for polishing. A rapid increase in polishing difficulty towards small focal ratios (as a third power of f/D) has been a major constraining factor for the former generation of telescopes with relatively slow primaries [8]†.

The technological revolution permitted by computer controlled polishing techniques and modern optical testing methods has made it possible to overcome limitations of the conventional techniques of the past. The amount of optical surface wavefront RMS misfigure achieved recently for large primary mirrors is only a small fraction of a micron. For the 1.8-m primary mirror of the Vatican telescope, RMS = 34 nm and δc = 8 [38]†, for the 1.1m secondary mirrors of the 8m Very Large Telescopes, RMS=15 nm and δc =30, for the 3.5m primary mirror of the Galileo telescope, RMS=16 nm and δ_c = 84 [39]†. For the 1.8m segments of the Keck I telescope, RMS = 16 nm and δc =32. These large mirrors possess the highest quality of optical surfaces yet produced, which demonstrates the recent remarkable progress in polishing techniques.

An extensive review of modern controlled figuring techniques is given in [40, and 41]†. The classical techniques with large and stiff polishing tools are used with an innovative modification, namely stress polishing. The workpiece is stressed by active support forces or bending moments in such a way that its surface can be figured spherical or flat. Deforming forces are chosen so that after being released the workpiece assumes the desired aspherical shape. This technique has been used for producing the off-axis hyperbolic segments of the Keck telescope projects.

Grinding and polishing processes affect the distribution of residual stresses within the workpiece, leading to uncontrolled surface warping which could exceed some microns after relaxation. A similar effect occurs in connection with the cutting segments into hexagons after the figuring process. In order to correct for such residual figure errors, Argon ion-beam polishing in a vacuum chamber is applied [42]†. This method is highly accurate and enables figure compensation to about 1 micron without degrading the microroughness.

The ability to measure the figure error during the fabrication process is a necessary feature for modern technology to deliver diffraction-limited quality of steep (f/1.0) aspheric mirrors.

1.8.5 Progress in Optical Testing of Large Mirrors

There are two principal testing methods for measuring the current mirror shape, optical [43]† and mechanical [44]†. Mechanical methods based on profilometer measurements are used at the initial and intermediate stages of the figuring process, since their precision is about one order of magnitude lower than that of optical test methods.

Interferometric testing methods with spherical test plates are not always possible because the deviation of an aspherical surface from the corresponding best-fit sphere can exceed hundreds of microns. For large mirrors, *autocollimation schemes* employing null lenses are used. In the presence of strong spherical aberration a *null system* provides stigmatic test conditions. A detailed description of optical test methods for aspherical mirrors is presented in [43, 45, 46]†.

Concave mirrors are effectively tested at the centre of curvature through null systems providing an autocollimation path. This means that after passing the null-lenses, the rays become normal to the optical surface being tested. Unfortunately, the null system is a potential source of errors during the test and therefore its quality needs crosschecking. Use of two independent null systems improves reliability of the test results. A crosscheck of the null-lens against a *computer generated hologram* (CGH), which mimics aberrations of the optical surface, enables easy verification of null system quality. In the modified scheme using CGH technology one can test off-axis aspherical segments [47]†.

The optical testing of large convex aspherical mirrors is most challenging, since it requires a compensator (glass matrix or Hindle sphere) at least as large as the mirror itself. A spherical matrix in the shape of a meniscus lens with a coated concentric hologram provides a means of testing convex aspherical mirrors using autocollimation schemes. This test method with a spherical matrix has been successfully demonstrated for the convex secondary mirrors of the LBT and the Magellan telescope [48]†. It should be noted that the ability of the optical test methods mentioned is such that it is possible to perform data sampling over entire surfaces in several hundred points with a precision in the range of a few nm.

1.9 The Aim of Thesis

The aim of this thesis is, first, to study how the asphericity factor effects the reflecting telescope parameters under investigation of this thesis. These parameters are:

1. the Δ-values (length segment from the tangent x-y plane to the surface);
2. ray aberrations both the transverse (TA) and the longitudinal (LA);
3. the angle the incident ray makes with the surface normal vector.

and second, to design a two-mirror reflecting telescope based upon this study.

The design fulfillments are 1m aperture (for comparison between surfaces of unified aperture), and 2.5m telescope (costless) with best possible features (light gathering power, and resolving power).

Chapter 2

Ray Tracing

2.1Ray Tracing

Ray tracing procedures are the mainstay and the mathematical tools essential for system evaluation before being constructed; because the obtained results are used in aberration calculations; and that's why it is of a fundamental importance in optical design. There are different types of ray tracing methods for the different types of the incoming rays. The programming work involved is skew ray tracing (exact ray tracing) through spherical surface and quadric surfaces of revolution (Cartesian surfaces).

Since the Gaussian region is a very small one in comparison with the total optical element (lens or mirror) size, especially, when large elements are used. Therefore, there is an insisting necessity to use more general procedure for tracing rays in three dimensions by using solid geometry instead of using paraxial ray tracing because it is just an approximation. So, the used procedure for such case takes into account the most general type of rays known as skew. The meaning of skew rays is those which are not co-planar with axis (optical axis) [18]. So, a skew ray must be defined in three coordinates x, y, and z. The only way to achieve further generality is to make use of this technique to get an exact analysis for ray tracing of such general case [6]. Figure (2.1) shows the diagram that illustrates the case of a skew ray.

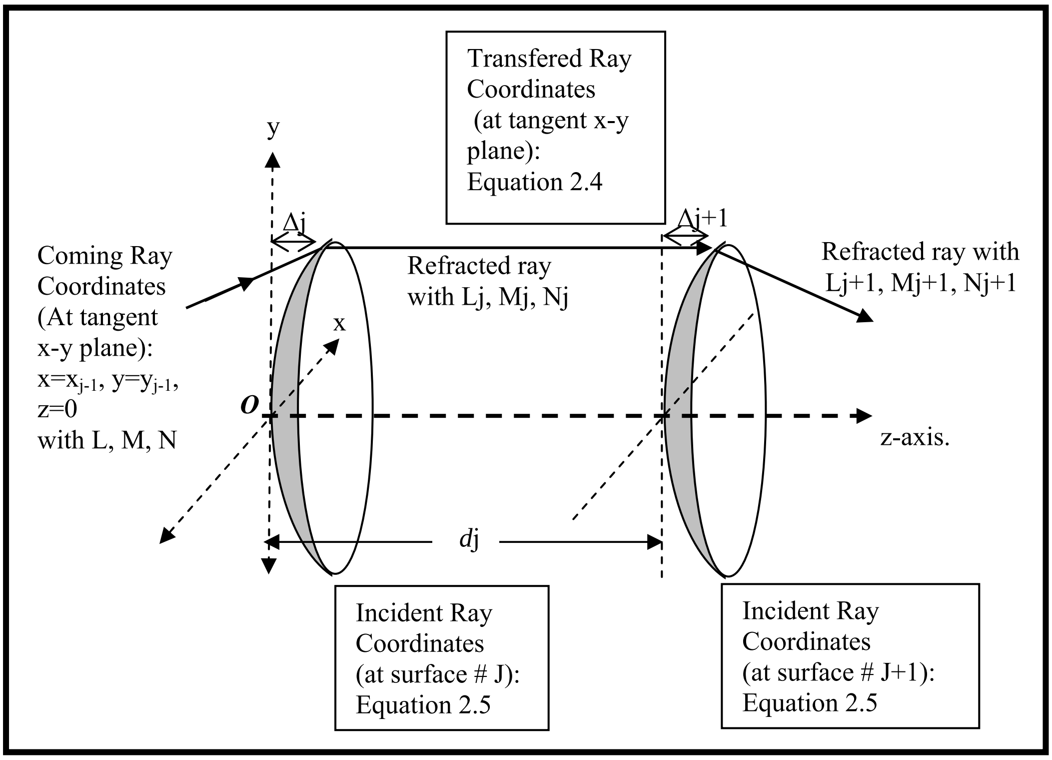

Figure (2.1) Geometry and notation used for tracing a skew ray between spherical surfaces.

2.2 Skew Ray Tracing through Spherical Surfaces

Before giving a flowchart that explains the programming work for a skew ray, exhibiting the used formulae is of great importance to illustrate the mathematical analysis for this case geometrically.

Lets consider the optical axis is a long the z-axis, passing through the (x-y) plane that are tangent to the surfaces of the optical elements from their vertices (figure 2.1). The starting equation that gives z–coordinates of a spherical surface is [19]:

$$z = \frac{c}{2}\left(x^2 + y^2 + z^2\right) \tag{2.1}$$

where c is the curvature of the surface, and x and y are the coordinates of the incident ray and the spherical surface.

To employ Snell’s law of the refraction in terms of geometrical forms, it has been reformulated as [19]:

$$\left.\begin{aligned} n'L' - nL &= k\alpha \\ n'M' - nM &= k\beta \\ n'N' - nN &= k\gamma \end{aligned}\right\} \tag{2.2}$$

where

$$k = n'\cos I' - n\cos I \tag{2.3}$$

L, *M*, and *N* are the direction cosines of the incident rays. α, β, and γ are the components of the unit normal at the point of incidence. The non–primed parameters belong to the previous medium. This method involves two sets of equations; the first for the transfer between spherical surface and the second for the refraction.

Transfer between Spherical Surfaces

The equations for transferring skew rays between spherical surfaces are [19]:

$$\left.\begin{aligned} x_0 &= x_{-1} + \frac{L}{N}\left(d - z_{-1}\right) \\ y_0 &= y_{-1} + \frac{M}{N}\left(d - z_{-1}\right) \end{aligned}\right\} \tag{2.4}$$

(x_{-1}, y_{-1}) are the coordinates of the coming ray, and (x_0, y_0) are the coordinates of the ray intersection with the (x–y) plane. The ray intersects the spherical surface in the coordinates are given by [19]:

$$\left.\begin{aligned} x &= x_0 + L\Delta \\ y &= y_0 + M\Delta \\ z &= N\Delta \end{aligned}\right\} \tag{2.5}$$

where Δ is the length segment from the (x–y) plane to the surface; which is expressed as [19]:

$$\Delta = \frac{F}{G + \sqrt{G^2 - cF}} \tag{2.6}$$

$$F = c\left(x_0^2 + y_0^2\right) \tag{2.7}$$

$$G = N - c\left(Lx_0 + My_0\right) \tag{2.8}$$

Refraction (Reflection) through Spherical Surfaces

It is important to refer that the expressions and notation used in this section for refraction are exactly the same expressions and notations used for reflection, taking into consideration that the angle of reflection is equal to the angle of incidence and the mirror index of refraction is equal to -1.

To obtain refraction (reflection) equations through spherical surface it is needed to know the components of the unit normal (. α, β, γ) at the point of incidence. These components can be obtained from [19]:

$$(\alpha, \beta, \gamma) = \frac{-\left(\dfrac{\partial F}{\partial x}, \dfrac{\partial F}{\partial y}, \dfrac{\partial F}{\partial z}\right)}{\sqrt{\left(\dfrac{\partial F}{\partial x}\right)^2 + \left(\dfrac{\partial F}{\partial y}\right)^2 + \left(\dfrac{\partial F}{\partial z}\right)^2}} \tag{2.9}$$

where F stands for equation (2.1). Using (2.9) in equation (2.2), the new values of the directional cosines (after refraction) can be expressed as [19]:

$$\left.\begin{aligned} n'L' &= nL - Kx \\ n'M' &= nM - Ky \\ n'N' &= nN - Kz + n'\cos I' - n\cos I \end{aligned}\right\} \tag{2.10}$$

where

$$K = c\left(n'\cos I' - n\cos I\right) \tag{2.11}$$

$$\cos I = \sqrt{G^2 - cF} \tag{2.12}$$

$$n'\cos I' = \sqrt{(n')^2 - n^2(1 - \cos^2 I)} \tag{2.13}$$

equations (2.10) up to (2.13) complete the refraction (reflection) process. Substituting the direction cosines of equation (2.10) in (2.4), the transfer process from one surface to another is done. After each refraction (reflection) process the direction cosines should be checked in order to assert the tracing validity. This can be done by [19]:

$$(L')^2 + (M')^2 + (N')^2 = 1 \tag{2.14}$$

The flowchart that explains the procedure used for skew ray tracing through spherical surfaces is shown in figure (2.2)

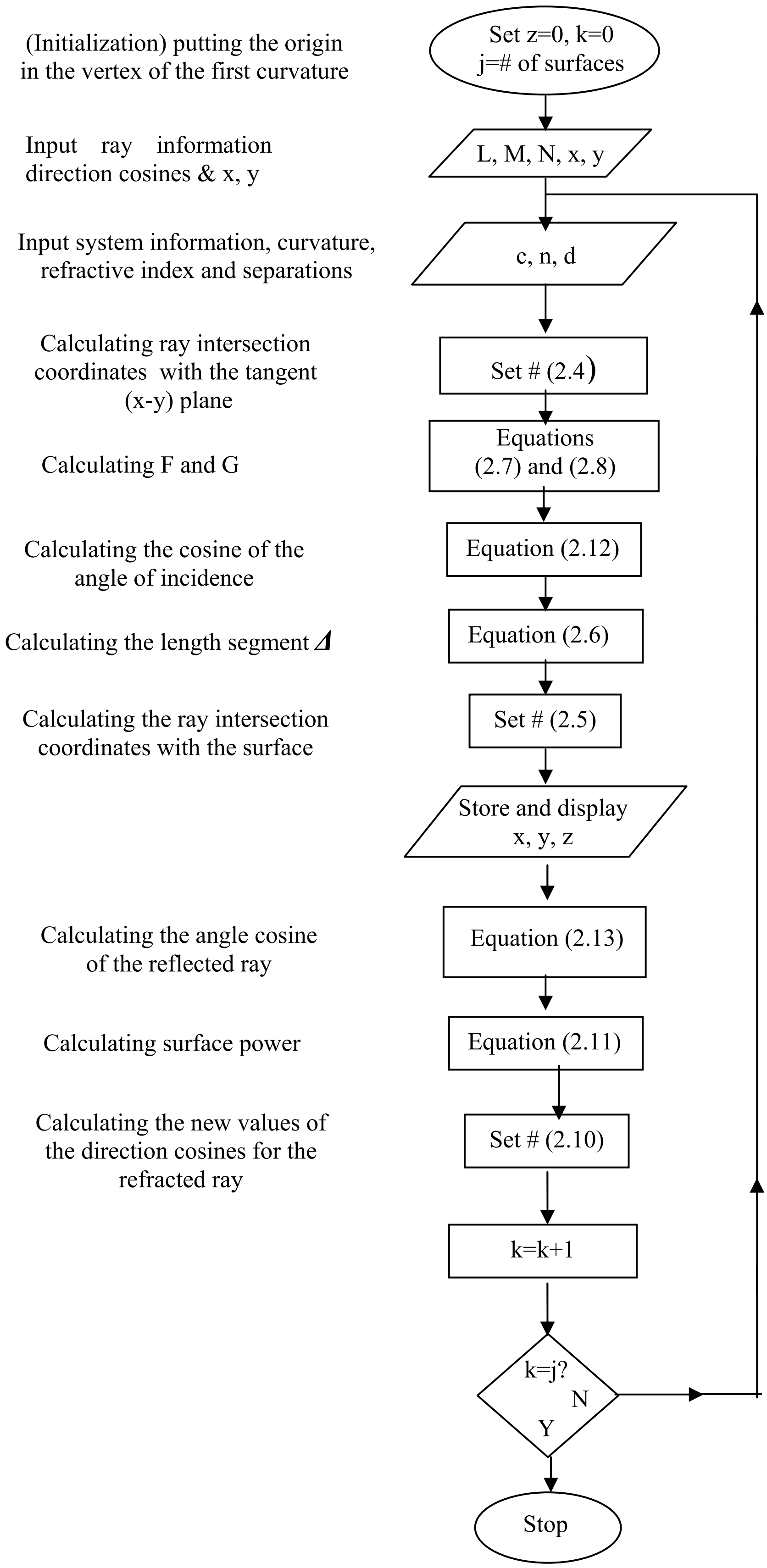

Figure (2.2) Flowchart for skew ray tracing through spherical surfaces.

2.3 Ray Tracing through Quadric of Revolution

Most optical surfaces are spherical because a spherical surface is the easiest to produce. However, non-spherical are necessary for some purposes, especially when they appear as the solution of particular optical problems, where one of these surfaces, ellipse, is the one that verifies Fermat's principle which states that the optical path length of each ray will be identical [5] . So, a code for tracing rays through aspherical surfaces is an essential and without such code, ray–tracing procedures are incomplete. With this code, ray–tracing procedures are suitable to trace rays through, approximately, all types of optical element surfaces.

For ray tracing purposes the equation used to represent the conic of revolution is [19]:

$$z = \frac{c}{2}\left(x^2 + y^2 + \varepsilon z^2\right) \tag{2.15}$$

This equation represents a surface of revolution about the z–axis, passing through the origin and having curvature c at that point. The parameter ε determines the asphericity as follows [19]:

$\varepsilon < 0$, hyperboloid

$\varepsilon = 0$, paraboloid

$0 < \varepsilon < 1$, prolate ellipsoid

$\varepsilon = 1$, sphere

$\varepsilon > 1$, oblate ellipsoid

The utility of equation (2.15) is to give a range for asphericities while keeping the paraxial curvature constant, which is essential in designing conic surfaces (Cartesian). The followed steps to trace rays through these surfaces are similar to those illustrated in the last section for skew rays between spherical surfaces.

Transfer between Quadrics

The transfer equations for the quadric are obtained by proceeding exactly the procedure for spherical surfaces given in §2.1 the only different formulae in this set is that for the length segment Δ, which is now expressed as (kindly, see the appendix):

$$\Delta = \frac{F}{G + \sqrt{G^2 - cF(1 + (\varepsilon - 1)N^2)}} \tag{2.16}$$

from equation (2.16), it is quite evident the result for a sphere (spherical surface) is recovered if ε is put equal to unity. The coordinates of ray intersection with the surface are obtained by using (2.16) in (2.5).

Refraction (Reflection) through Quadric

Refraction (reflection) calculations must again be restarted from finding the cosine of the angle of incidence; by applying equation (2.9) to equation (2.15) to obtain the direction cosines of the normal as (kindly, see the appendix):

$$\left.\begin{aligned}
\alpha &= \frac{-cx}{\sqrt{1 - 2c(\varepsilon - 1)z + c^2\varepsilon(\varepsilon - 1)z^2}} \\
\beta &= \frac{-cy}{\sqrt{1 - 2c(\varepsilon - 1)z + c^2\varepsilon(\varepsilon - 1)z^2}} \\
\gamma &= \frac{1 - c\varepsilon z}{\sqrt{1 - 2c(\varepsilon - 1)z + c^2\varepsilon(\varepsilon - 1)z^2}}
\end{aligned}\right\} \tag{2.17}$$

The cosine of the angle of incidence cos$I$ can be obtained by the scalar multiplication with the direction cosines of the ray tracing, it is expressed as (kindly, see the appendix):

$$\cos I = \frac{N - c(Lx + My + N\varepsilon z)}{\sqrt{1 - 2c(\varepsilon - 1)z + c^2\varepsilon(\varepsilon - 1)z^2}} \tag{2.18}$$

Refraction (reflection) calculations are completed by using equation (2.13), (2.3), and (2.2) respectively. The condition (equation 2.14) of direction cosines can be used for the same purposes as before. The new values of the direction cosines of the refracted (reflected) ray should be substituted in equation (2.4) to complete the transfer process from one surface to another.

The flowchart that explains the procedure used for skew ray tracing through quadric surfaces is shown in figure (2.3)

In order to identify my personal contribution to the formulation of the skew ray tracing, equations 2.16, 2.17, and 2.18 have been reformulated. This reformulation is based upon analytical derivation to these formulas by using the same notation of [19], (kindly see the appendix).

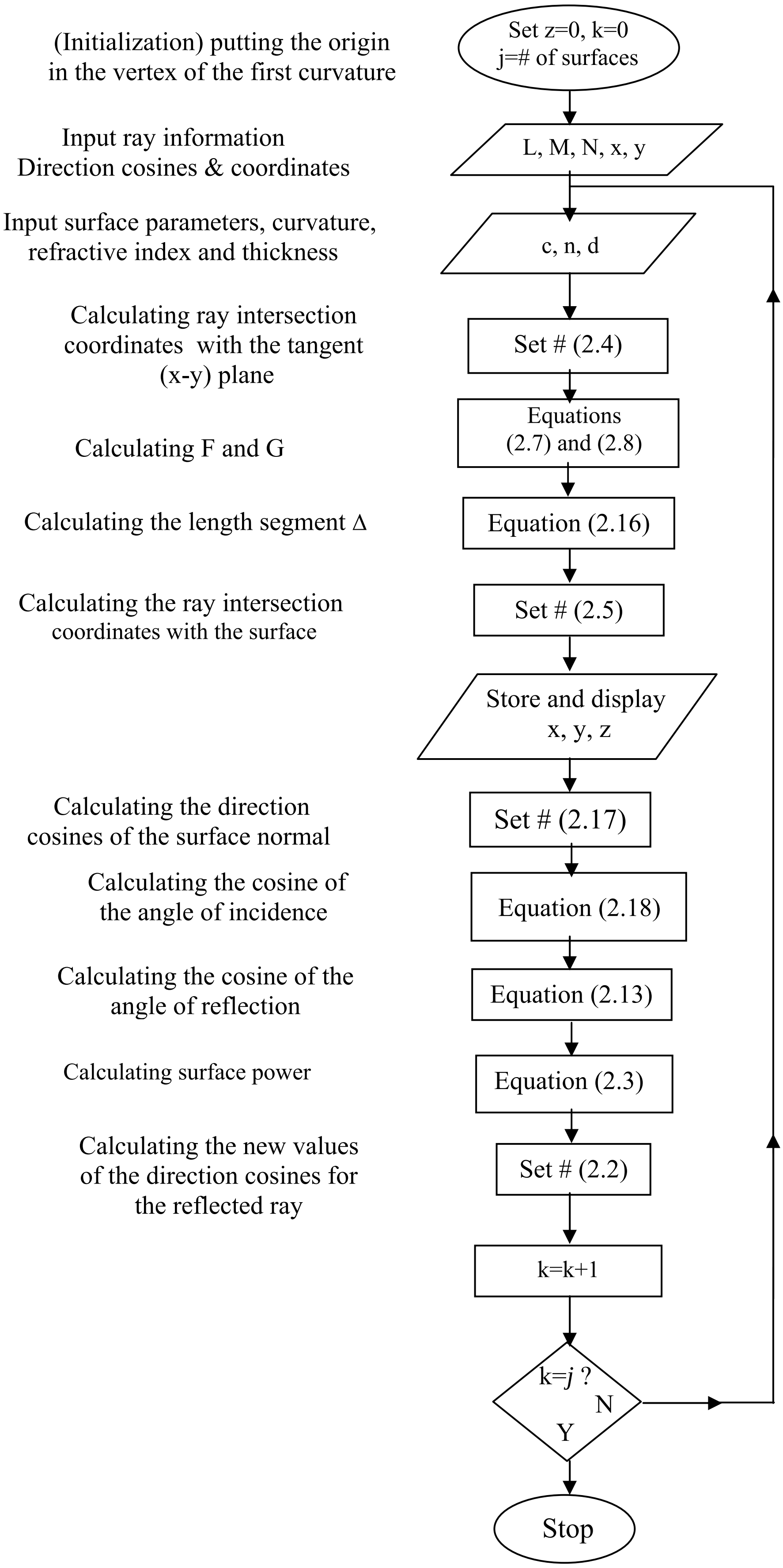

Figure (2.3) Flowchart for ray tracing through conic surfaces.

2.4 Computing Transverse (TA) and Longitudinal (LA) Aberrations

This section exhibits the expressions used to compute the results of TA, and LA in Chapter 3. Concerning TA results, they computed by using one of the skew ray tracing equations (equation2.4):

$$y_o = y_{-1} + \frac{M}{N}\left(f - z_{-1}\right) \qquad (2.19)$$

In this equation, y_o stands for TA, where y_o is the incident ray height at the focal plane of the optical element(mirror), y_{-1} is the ray height in the previous surface (mirror surface), N, and M are the ray direction cosines, $f\,l$ is the mirror focal length, and z_{-1} is the length segment from the(x-y) plane tangent to the surface(mirror).

Concerning LA results, they computed by using the following equation

$$LA = \frac{TA}{\tan(convergence\ angle)} \qquad (2.20)$$

where $\text{convergence} = 2 \times \text{angle of reflection}$

Since the angle of reflection is equal to the incident angle, thus it can be obtained from equation 2.18

$$\cos I = \frac{N - c(Lx + My + N\varepsilon z)}{\sqrt{1 - 2c(\varepsilon - 1)z + c^2\varepsilon(\varepsilon - 1)z^2}}$$

The angle values (I)computers display are in radian, and those displayed in degrees in chapter three are obtained by:

$$\text{Angle} = \frac{\text{I} \times 180}{\pi} \qquad (2.21)$$

Chapter 3

Results & Discussion

First of all, before setting off to discuss the results of figures and tables, it is very important to refer that all the results appear in this chapter are based upon considering the surfaces (mirrors) of 5m radius of curvature (R=500cm). This means that the paraxial curvature (*c, where c=1/R*) is kept invariant (constant) in all mirrors. Keeping the paraxial curvature *c* constant is very essential for two reasons (keeping the paraxial curvature constant, which is essential in designing conic surfaces [19]):

1. It is difficult to compare, judge, and select the proper type of surfaces (mirrors) to represent a telescope mirrors unless all surfaces have the same paraxial curvature.
2. To study the effect of the asphericity factor ε on the parameters of the reflecting surfaces, the paraxial curvature is kept constant. This is because mirrors are single-surface optical elements with no thickness parameter; while lenses have two surfaces and thickness. So, in the case of mirrors there is only one and unique optical design parameter that controls mirrors performance (focal length and magnification); it is the paraxial curvature *c*.

3.1 Discussing Surfaces' Shapes

It is important, here, to refer that the considered aperture used to achieve the task of this section is 9m (900cm) aperture except the case of oblate ellipsoid; where the considered aperture is 1m. In this section the effect of changing the asphericitry factor (ε) on the shapes of quadric (conic or Cartesian) surfaces will be discussed. This task achieved exhibiting the Δ-values of those surfaces (along the optical axis) versus the aperture diameter. The aperture diameter of the surface is represented as the height (y in cm) of the incident light ray on these surfaces. The Δ-values of these surfaces represent, in skew ray tracing procedure, the length segment from the plane that passes through the optical axis(z-axis) and tangent to the surface at the origin (surface vertex), so the ray height axis (aperture diameter axis) can represent the tangent x-y plane. The actual Δ-values those listed in the tables have negative sign, because the length segment from the tangent x-y plane to mirrors' surfaces is from right to left, and according to the sign convention these values are negative. But figures from 3.1 up to 3.4, exhibited Δ-values as positive when plotted against the ray height values just to compare between one figure and another.

The asphericity factor (ε) factor changes the shapes of quadric surfaces. Figures 3.1, 3.2, 3.3, and 3.4 obviously clear this fact. These figures exhibit the Δ-values of these surfaces versus the ray height or the aperture diameter, where the Δ- axis represents the optical axis.

Figure 3.1 shows the effect of decreasing (ε) on the shapes of surfaces in the region of hyperboloid (ε<0). In the interval [-100,100]cm along the aperture diameter axis, the surfaces curves seem to coincide. Beyond this interval the surfaces begin to depart from each other. This figure also shows that as ε=-0.01 the surface shape is very close to that of paraboloid and as ε decreases down to ε=-1000 the shapes become more and more flattened. In other words, it means that the Δ -values begin to become closer and closer to the plane tangent to the surface at its vertex.

Geometrically (in terms of skew ray tracing), this means that the length segment between a point on a surface and the tangent plane is getting smaller and smaller as (ε) decreases from ε=-0.1 down to ε=-1000, (kindly, see table 3.1) consequently, this behavior leads to the conclusion that when $\varepsilon = -\infty$ the surface becomes plane.

Figure 3.2 compares between the shape of spherical surface (ε=1) and the shape of the paraboloid (ε=0). The Δ-values of both seems to coincide for a while or interval of aperture diameter [-250,250] cm. beyond this interval the Δ-values those belong to the spherical surface begin to show higher response to the increase in aperture diameter as they get higher Δ-values for the same aperture diameter. Geometrically, this means that the length segment between a point on a spherical surface and the tangent plane is larger than the length segment between a point on the surface of paraboloid and the tangent plane(kindly, see table 3.2).

Figure 3.3 shows how ε works in the region of prolate ellipsoid ($0<\varepsilon<1$), this is very clear that the shapes of prolate ellipsoid ε forms are ranging between paraboloid (ε=0) and spherical surface (ε=1). When ε=0.2 the surface shape is very close to that of paraboloid and when ε=0.8 the surface shape is very close to that of spherical surface (kindly, see table 3.2).

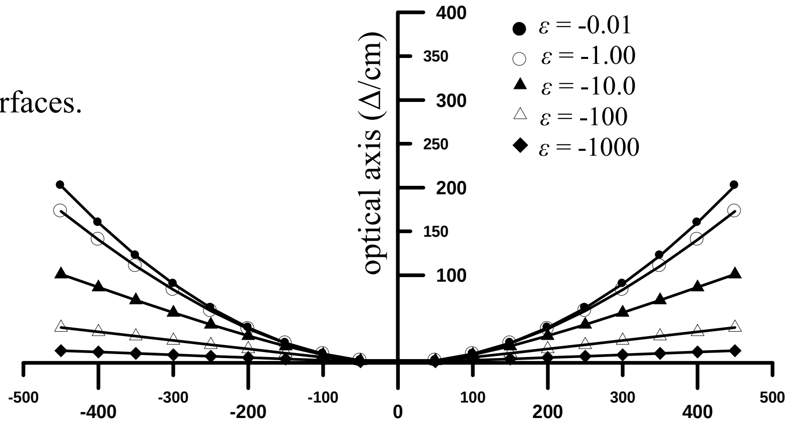

Fig. 3.1 hyperboloid surfaces.

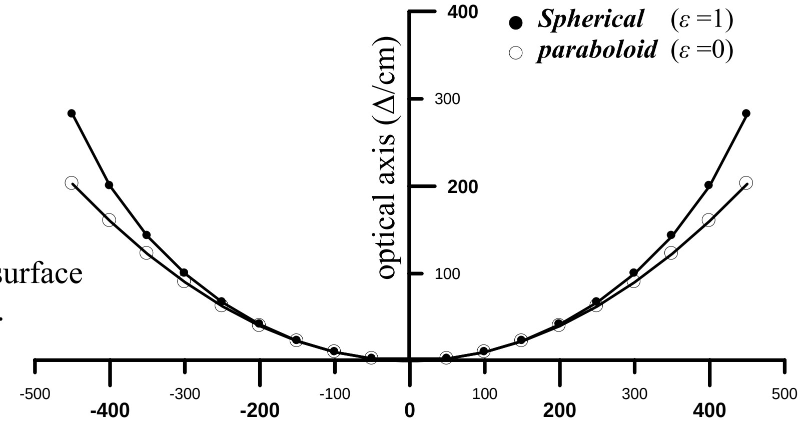

Fig. 3.2 Spherical surface & paraboloid.

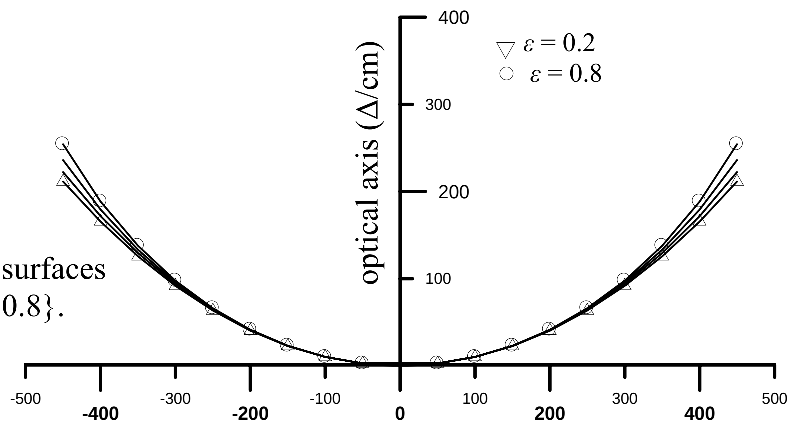

Fig. 3.3 Prolate ellipsoid surfaces for ε={0.2, 0.4, 0.6, 0.8}.

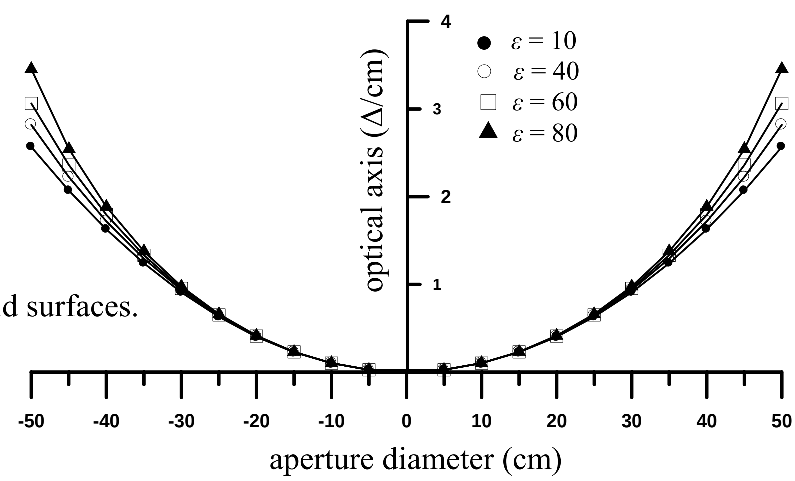

Fig. 3.4 Oblate ellipsoid surfaces.

Figure 3.4 shows the influence of increasing ε in the region of oblate ellipsoid (ε>1). In this region, the case is quite the contrast to that for hyperboloid; the story of Δ-values response to the aperture diameter in the comparison between spherical surface and paraboloid is going on but with higher response. The previous figures 3.1, 3.2, and 3.3, the domain of the aperture diameter was [-500cm, 500cm] to get a noticeable change in Δ-values (shape of the surfaces). While in this case, the domain of the aperture diameter is [-50, 50]cm due to the higher response the Δ-values showed versus the increase in ε. (kindly, see table 3.3)

Table 3.1 Δ- values versus the ray heights forming hyperboloids surfaces of 500 cm radii.

	Δ(cm)				
y(cm)	***ε*** **=-1000**	***ε*** **=-100**	***ε*** **=-10**	***ε*** **=-1**	***ε*** **=-0.01**
450	-13.73903	-40.27693	-100.831	-172.6812	-202.0916
400	-12.15899	-35.31129	-86.0147	-140.3124	-159.7448
350	-10.57926	-30.35534	-71.44958	-110.3278	-122.3503
300	-9	-25.41381	-57.23806	-83.09519	-89.91915
250	-7.42149	-20.4951	-43.54144	-59.017	-62.46099
200	-5.844289	-15.61553	-30.62258	38.51648	-39.98401
150	-4.269696	-10.81139	-18.92024	-22.01533	-22.49494
100	-2.701562	-6.18034	-9.160798	-9.901952	-9.999001
50	-1.158312	-2.071068	-2.440442	-2.493781	-2.499938
-50	-1.158312	-2.071068	-2.440442	-2.493781	-2.499938
-100	-2.701562	-6.18034	-9.160798	-9.901952	-9.999001
-150	-4.269696	-10.81139	-18.92024	-22.01533	-39.98401
-200	-5.844289	-15.61553	-30.62258	-38.51648	-62.46099
-250	-7.42149	-20.4951	-43.54144	-59.017	-89.91915
-300	-9	-25.41381	-57.23806	-83.09519	-122.3503
-350	-10.57926	-30.35534	-71.44958	-110.3278	-202.0916
-400	-12.15899	-35.31129	-86.0147	-140.3124	-159.7448
-450	-13.73903	-40.27693	-100.831	-172.6812	-202.0916

Table 3.2 **Δ**- values versus the ray heights forming paraboloid, prolate ellipsoid surfaces, and spherical surface, all of 500 cm radius.

	Δ(cm)					
	Paraboloid	**Prolate ellipsoid**				**Sphere**
Y(cm)	**(ε=0)**	**(ε=0.2)**	**(ε=0.4)**	**(ε=0.6)**	**(ε=0.8)**	**(ε=1)**
450	-202.5	-211.4415	-222.2598	-235.8851	-254.1901	-282.0551
400	-160	-165.4765	-171.8071	-179.2861	-188.3938	-200
350	-122.5	-125.658	-129.1744	-133.135	-137.6603	-142.9286
300	-90.00001	-91.68109	-93.49666	-95.46855	-97.62444	-100
250	-62.5	-63.30142	-64.14588	-65.03796	-65.98301	-66.9873
200	-40	-40.32523	-40.66134	-41.00904	-41.36913	-41.74243
150	-22.5	-22.60217	-22.70623	-22.81224	-22.92027	-23.0304
100	-10	-10.02008	-10.04032	-10.06073	-10.08131	-10.10205
50	-2.5	-2.501251	-2.502505	-2.503761	-2.50502	-2.506281
-50	-2.5	-2.501251	-2.502505	-2.503761	-2.50502	-2.506281
-100	-10	-10.02008	-10.04032	-10.06073	-10.08131	-10.10205
-150	-22.5	-22.60217	-22.70623	-22.81224	-22.92027	-23.0304
-200	-40	-40.32523	-40.66134	-41.00904	-41.36913	-41.74243
-250	-62.5	-63.30142	-64.14588	-65.03796	-65.98301	-66.9873
-300	-90.00001	-91.68109	-93.49666	-95.46855	-97.62444	-100
-350	-122.5	-125.658	-129.1744	-133.135	-137.6603	-142.9286
-400	-160	-165.4765	-171.8071	-179.2861	-188.3938	-200
-450	-202.5	-211.4415	-222.2598	-235.8851	-254.1901	-282.0551

Table 3.3 Δ- values versus the ray heights forming oblate ellipsoid surfaces of 500 cm radii.

	Δ(cm)				
y(cm)	**(ε=10)**	**(ε=20)**	**(ε=40)**	**(ε=60)**	**(ε=80)**
50	-2.565835	-2.63932	-2.817542	-3.062871	-3.454915
45	-2.067756	-2.114415	-2.222598	-2.358851	-2.541901
40	-1.626454	-1.654765	-1.718071	-1.792861	-1.883938
35	-1.240386	-1.25658	-1.291744	-1.331349	-1.376603
30	-0.9082492	-0.9168109	-0.9349665	-0.9546855	-0.9762443
25	-0.6289558	-0.6330141	-0.6414587	-0.6503796	-0.65983
20	-0.4016129	-0.4032522	-0.4066134	-0.4100904	-0.4136913
15	-0.2255086	-0.2260217	-0.2270623	-0.2281224	-0.2292027
10	-0.1001002	-0.1002008	-0.1004032	-0.1006073	-0.1008131
-10	-0.1001002	-0.1002008	-0.1004032	-0.1006073	-0.1008131
-15	-0.2255086	-0.2260217	-0.2270623	-0.2281224	-0.2292027
-20	-0.4016129	-0.4032522	-0.4066134	-0.4100904	-0.4136913
-25	-0.6289558	-0.6330141	-0.6414587	-0.6503796	-0.65983
-30	-0.9082492	-0.9168109	-0.9349665	-0.9546855	-0.9762443
-35	-1.240386	-1.25658	-1.291744	-1.331349	-1.376603
-40	-1.626454	-1.654765	-1.718071	-1.792861	-1.883938
-45	-2.067756	-2.114415	-2.222598	-2.358851	-2.541901
-50	-2.565835	-2.63932	-2.817542	-3.062871	-3.454915

3.2 Discussing the Telescope's Parameters

In this section, all the considered surfaces (mirrors) are of D=1m aperture diameter (-50cm≤y≤ 50cm), and R=5m radius of curvature for selecting the surface with best features to stand for the primary mirror.

This section discusses the effect of changing the shapes of surfaces, due to varying ε, on the reflecting telescope parameters under investigation of the project of this thesis. These parameters are:

1. The length segment Δ–values.
2. The angle (in degrees)the incident ray makes with the normal to the surface at the point of incidence. It is necessary to mention, here, that this angle determines the power of surface for each individual ray height (y-coordinates in cm). So, different angles give different powers (focal length or magnification) and this leads to (the two following parameters)rays aberrations.
3. Longitudinal Aberrations (LA), directly related to the distance, ray makes when intersects the optical axis, before or behind the focus.
4. The Transverse Aberrations (TA) which refers to the distance above or below the optical axis to the ray intersection with the focal plane.

Table 3.4 for spherical surface (ε=1)shows that the length segment (Δ-values) from the tangent plane to the surface increases from 0.10001cm to 2.50628cm when the ray height (y in cm) varies from 10cm to 50cm away from the optical axis. This was associated with angle variation, the angle the incident ray makes with the vector normal to surface, from 1.14603^{o} to 5.739^{o} to the same interval of ray height. This, in turn, changed the power of the surface along the aperture for each individual ray height, and then the appearance of TA as consequent. The marginal rays (y=50cm and y=-50cm) produce TA =0.225cm and -0.255cm respectively. As shown in the table the rays above the optical axis intersect the focal plane below the focal point and the rays below the optical axis intersects the focal plane above the focal point. And this means that the rays in the case of spherical surfaces (ε=1) intersect the optical axis before the paraxial focal point which justifies the positive values for the LA (maximum value for LA=1.259cm).

Table 3.4 Results of 500cm radius, 100cm aperture diameter spherical mirror (ε=1).

Y(cm)	z(cm)	Angle(^{o})	LA(cm)	TA(cm)	$L^2+M^2+N^2$
50	-2.506281	5.739176	1.259664	-0.2557378	1
45	-2.029117	5.163612	1.018917	-0.1856209	1
40	-1.602568	4.588554	0.803224	-0.1298644	1
35	-1.226504	4.014004	0.6157961	-8.669955e-2	1
30	-0.9008115	3.4398	0.4503085	-0.0544386	1
25	-0.6253911	2.866008	0.3152064	-3.142375e-2	1
20	-0.4001601	2.29243	0.1988541	-1.605671e-2	1
15	-0.2250507	1.71908	0.1051648	-6.761057e-3	1
10	-0.10001	1.14603	5.823889e-2	-2.00056e-3	1
-10	-0.10001	1.14603	5.823889e-2	2.00056e-3	1
-15	-0.2250507	1.71908	0.1051648	6.761057e-3	1
-20	-0.4001601	2.29243	0.1988541	1.605671e-2	1
-25	-0.6253911	2.866008	0.3152064	3.142375e-2	1
-30	-0.9008115	3.4398	0.4503085	0.0544386	1
-35	-1.226504	4.014004	0.6157961	8.669955e-2	1
-40	-1.602568	4.588554	0.803224	0.1298644	1
-45	-2.029117	5.163612	1.018917	0.1856209	1
-50	-2.506281	5.739176	1.259664	0.2557378	1

Table 3.5 for paraboloid (ε=0) shows that the length segment from the tangent plane to the surface (Δ-values) varies from 0.1cm to 2.5cm when the ray height varies from 10cm to 50cm. For the same interval of y the table shows variation in the angle from 1.14589^o to 5.710623^o. A comparison between the results in table 3.4 and 3.5 shows that the difference in the Δ-values for the marginal ray is 0.006cm or 60μm and difference between the angles those rays made is 0.003^o which are very fine. But these very fine differences yield a complete elimination to spherical aberrations; since $1cm\times10^{-7}$=1nm. Thus, 97nm (highest TA value) is much less than that of the visible region (400nm< λ <700nm).

Table 3.5 Results of 500cm radius, 100cm aperture diameter paraboloid mirror (ε=0).

y(cm)	z(cm)	Angle(^{o})	LA(cm)	TA(cm)	$L^2+M^2+N^2$
50	-2.5	5.710623	-2.4749867e-6	5.00e-7	0.9999995
45	-2.025	5.142737	-8.5303867e-6	15.48e-7	1
40	-1.6	4.573932	-6.4583845e-6	10.40e-7	0.9999998
35	-1.225	4.004186	-38.986467e-6	54.85e-7	0.9999999
30	-0.9	3.433648	-81.040113e-6	97.60e-7	0.9999998
25	-0.625	2.862386	-66.084821e-6	66.25e-7	1
20	-0.4	2.290551	-15.974813e-6	12.80e-7	1
15	-0.225	1.718397	-35.950130e-6	21.59e-7	0.9999999
10	-0.1	1.145859	-39.980640e-6	16.0e-7	0.9999997
-10	-0.1	1.145859	-39.980640e-6	-16.0e-7	0.9999997
-15	-0.225	1.718397	-35.950130e-6	-21.59e-7	0.9999999
-20	-0.4	2.290551	-15.974813e-6	-12.80e-7	1
-25	-0.625	2.862386	-66.084821e-6	-66.25e-7	1
-30	-0.9	3.433648	-81.040113e-6	-97.60e-7	0.9999998
-35	-1.225	4.004186	-38.986467e-6	-54.85e-7	0.9999999
-40	-1.6	4.573932	-6.4583845e-6	-10.40e-7	0.9999998
-45	-2.025	5.142737	-8.5303867e-6	-15.48e-7	1
-50	-2.5	5.710623	-2.4749867e-6	-5.00e-7	0.9999995

Tables 3.6, 3.7, 3.8, and 3.9 (for prolate ellipsoid); these tables show that their results are ranging between those in the case of paraboloid and the case of spherical surface. It is very clear that when ε=0.2 (table3.6) the results are very close to those of paraboloid (ε=0) and when ε=0.8 (table3.9) the results are close to those of spherical surface (ε=1), and when ε=0.4 and ε=0.6 the results are in between.

Table 3.6 Results of 500cm radius, 100cm aperture diameter prolate ellipsoid mirror of ε=0.2

y(cm)	z(cm)	Angle(^{o})	LA(cm)	TA(cm)	L^2+M^2 +N^2
50	-2.501251	5.716318	0.2532806	-5.084326e-2	0.9999995
45	-2.025821	5.146888	0.2021759	-3.694014e-2	1
40	-1.600512	4.576799	0.1583835	-2.587078e-2	1
35	-1.2253	4.006191	0.1266284	-0.0172962	0.9999994
30	-0.9001621	3.434902	9.292567e-2	-1.086728e-2	0.9999996
25	-0.6250781	2.86307	5.817991e-2	-6.272856e-3	1
20	-0.400032	2.290978	4.026034e-2	-3.207913e-3	0.9999999
15	-0.2250101	1.718397	5.68749e-3	-0.0013494	1
10	-0.100002	1.145859	2.095442e-2	-4.005632e-4	0.9999998
-10	-0.100002	1.145859	2.095442e-2	4.005632e-4	0.9999998
-15	-0.2250101	1.718397	5.68749e-3	0.0013494	1
-20	-0.400032	2.290978	4.026034e-2	3.207913e-3	0.9999999
-25	-0.6250781	2.86307	5.817991e-2	6.272856e-3	1
-30	-0.9001621	3.434902	9.292567e-2	1.086728e-2	0.9999996
-35	-1.2253	4.006191	0.1266284	0.0172962	0.9999994
-40	-1.600512	4.576799	0.1583835	2.587078e-2	1
-45	-2.025821	5.146888	0.2021759	3.694014e-2	1
-50	-2.501251	5.716318	0.2532806	5.084326e-2	0.9999995

Table 3.7 Results of 500cm radius, 100cm aperture diameter prolate ellipsoid mirror of ε=0.4

y(cm)	z(cm)	Angle(^{o})	LA(cm)	TA(cm)	L^2+M^2 +N^2
50	-2.502505	5.721972	0.5029576	-0.1018295	1
45	-2.026643	5.151113	0.4089954	-7.398331e-2	0.9999995
40	-1.601025	4.579795	0.3230317	-0.0517997	0.9999996
35	-1.225601	4.008048	0.2430423	-0.0345981	1
30	-0.9003243	3.436099	0.1803337	-2.174047e-2	0.9999999
25	-0.6251563	2.863822	0.1240197	-1.255654e-2	1
20	-0.400064	2.291406	8.696601e-2	-6.421361e-3	0.9999996
15	-0.2250203	1.718739	0.0554668	-2.70465e-3	0.9999997
10	-0.100004	1.14603	0.0582449	-8.016349e-4	0.9999995
-10	-0.100004	1.14603	0.0582449	8.016349e-4	0.9999995
-15	-0.2250203	1.718739	0.0554668	2.70465e-3	0.9999997
-20	-0.400064	2.291406	8.696601e-2	6.421361e-3	0.9999996
-25	-0.6251563	2.863822	0.1240197	1.255654e-2	1
-30	-0.9003243	3.436099	0.1803337	2.174047e-2	0.9999999
-35	-1.225601	4.008048	0.2430423	0.0345981	1
-40	-1.601025	4.579795	0.3230317	0.0517997	0.9999996
-45	-2.026643	5.151113	0.4089954	7.398331e-2	0.9999995
-50	-2.502505	5.721972	0.5029576	0.1018295	1

Table 3.8 Results of 500cm radius, 100cm aperture diameter prolate ellipsoid mirror of ε=0.6

y(cm)	z(cm)	Angle(°)	LA(cm)	TA(cm)	$L^2+M^2+N^2$
50	-2.503761	5.727655	0.7534409	-0.1529703	1
45	-2.027467	5.155257	0.611541	-0.1111	0.9999998
40	-1.601539	4.582745	0.4849783	-7.777584e-2	0.9999994
35	-1.225902	4.01005	0.3684891	-5.194262e-2	1
30	-0.9004866	3.437352	0.2717851	-0.0326285	0.9999999
25	-0.6252345	2.864505	0.1838017	-1.883985e-2	1
20	-0.4000961	2.291747	0.124257	-9.631894e-3	0.9999998
15	-0.2250304	1.718853	7.204297e-2	-4.056463e-3	0.9999999
10	-0.100006	1.145859	2.095042e-2	-1.200729e-3	1
-10	-0.100006	1.145859	2.095042e-2	1.200729e-3	1
-15	-0.2250304	1.718853	7.204297e-2	4.056463e-3	0.9999999
-20	-0.4000961	2.291747	0.124257	9.631894e-3	0.9999998
-25	-0.6252345	2.864505	0.1838017	1.883985e-2	1
-30	-0.9004866	3.437352	0.2717851	0.0326285	0.9999999
-35	-1.225902	4.01005	0.3684891	5.194262e-2	1
-40	-1.601539	4.582745	0.4849783	7.777584e-2	0.9999994
-45	-2.027467	5.155257	0.611541	0.1111	0.9999998
-50	-2.503761	5.727655	0.7534409	0.1529703	1

Table 3.9 Results of 500cm radius, 100cm aperture diameter prolate ellipsoid mirror of ε=0.8

y(cm)	z(cm)	Angle(°)	LA(cm)	TA(cm)	$L^2+M^2+N^2$
50	-2.50502	5.733401	1.00618	-0.2042748	1
45	-2.028291	5.159398	0.8136125	-0.1483158	1
40	-1.602053	4.585608	0.6419042	-0.1037858	1
35	-1.226203	4.011954	0.4876491	-6.930795e-2	1.000001
30	-0.900649	3.438548	0.3590099	-4.352804e-2	1
25	-0.6253128	2.865257	0.2495499	-2.513105e-2	1
20	-0.4001281	2.292089	0.1615784	-0.0128443	0.9999999
15	-0.2250405	1.718967	8.860388e-2	-5.41014e-3	1
10	-0.100008	1.14603	0.0582409	-1.601801e-3	0.9999997
-10	-0.100008	1.14603	0.0582409	1.601801e-3	0.9999997
-15	-0.2250405	1.718967	8.860388e-2	5.41014e-3	1
-20	-0.4001281	2.292089	0.1615784	0.0128443	0.9999999
-25	-0.6253128	2.865257	0.2495499	2.513105e-2	1
-30	-0.900649	3.438548	0.3590099	4.352804e-2	1
-35	-1.226203	4.011954	0.4876491	6.930795e-2	1.000001
-40	-1.602053	4.585608	0.6419042	0.1037858	1
-45	-2.028291	5.159398	0.8136125	0.1483158	1
-50	-2.50502	5.733401	1.00618	0.2042748	1

Tables 3.10, 3.11, 3.12, and 3.13 (for oblate ellipsoid), show that for the set of ε = {20, 40, 60, 80}there is a set of Δ= {-2.63932, -2.817542, -3.062871, -3.454915} cm, and for the same interval of asphericity factor the angles' set={6.379349°, 7.356153°, 8.984894°, 12.60439°} when the ray height y=50cm. So, it is clear that increasing ε leads to increase both Δ-values and the angle the incident ray makes with normal. And, as consequent, there is increase in aberrations (TA and LA) over those of spherical mirror of the same paraxial curvature as ε increases. For the same set of ε above the sets of TA and LA are, respectively, {-6.011672, -14.90397, -30.09065, -66.06139} and {26.54819, 56.76044, 92.77639, 140.3319}. The signs of TA and LA refer that the power of the mirror increased with increasing ε. So, it is concluded that, the ray above the optical axis intersected the focal plane below the optical axis and vise versa. And that's why the LA has positive values, since all rays intersects the optical axis before the paraxial focal length.

Table 3.10 Results of 500cm radius, 100cm aperture diameter oblate ellipsoid mirror of ε=20

y(cm)	z(cm)	Angle(^{o})	LA(cm)	TA(cm)	$L^2+M^2+N^2$
50	-2.63932	6.379349	26.54819	-6.011672	1
45	-2.114415	5.614995	21.24168	-4.21755	1
40	-1.654765	4.89657	16.60451	-2.866372	1
35	-1.25658	4.215332	12.59848	-1.86736	1
30	-0.9168109	3.564033	9.186903	-1.148687	0.9999999
25	-0.6330141	2.93665	6.339413	-0.6520168	0.9999999
20	-0.4032522	2.328097	4.033119	-0.3287014	1
15	-0.2260217	1.734042	2.263602	-0.137038	0.9999999
10	-0.1002008	1.150291	0.9845008	-4.026527e-2	1
-10	-0.1002008	1.150291	0.9845008	4.026527e-2	1
-15	-0.2260217	1.734042	2.263602	0.137038	0.9999999
-20	-0.4032522	2.328097	4.033119	0.3287014	1
-25	-0.6330141	2.93665	6.339413	0.6520168	0.9999999
-30	-0.9168109	3.564033	9.186903	1.148687	0.9999999
-35	-1.25658	4.215332	12.59848	1.86736	1
-40	-1.654765	4.89657	16.60451	2.866372	1
-45	-2.114415	5.614995	21.24168	4.21755	1
-50	-2.63932	6.379349	26.54819	6.011672	1

Table 3.11 Results of 500cm radius, 100cm aperture diameter oblate ellipsoid mirror of ε=40

y(cm)	z(cm)	Angle(^{o})	LA(cm)	TA(cm)	$L^2+M^2+N^2$
50	-2.817542	7.356153	56.76044	-14.90397	1
45	-2.222598	6.246953	44.69329	-9.903011	0.9999995
40	-1.718071	5.298903	34.49854	-6.454811	0.9999999
35	-1.291744	4.463877	25.90908	-4.070153	1
30	-0.9349665	3.710457	18.73611	-2.440494	1
25	-0.6414587	3.016945	12.84521	-1.357915	1
20	-0.4066134	2.367529	8.137897	-0.6741723	1
15	-0.2270623	1.750106	4.540058	-0.2779032	1
10	-0.1004032	1.155044	2.009765	- 8.102299e-2	0.9999999
-10	-0.1004032	1.155044	2.009765	8.102299e-2	0.9999999
-15	-0.2270623	1.750106	4.540058	0.2779032	1
-20	-0.4066134	2.367529	8.137897	0.6741723	1
-25	-0.6414587	3.016945	12.84521	1.357915	1
-30	-0.9349665	3.710457	18.73611	2.440494	1
-35	-1.291744	4.463877	25.90908	4.070153	1
-40	-1.718071	5.298903	34.49854	6.454811	0.9999999
-45	-2.222598	6.246953	44.69329	9.903011	0.9999995
-50	-2.817542	7.356153	56.76044	14.90397	1

Table 3.12 Results of 500cm radius, 100cm aperture diameter oblate ellipsoid mirror of ε=60.

y(cm)	z(cm)	Angle(^{o})	LA(cm)	TA(cm)	$L^2+M^2+N^2$
50	-3.062871	8.984894	92.77639	-30.09065	0.9999996
45	-2.358851	7.155109	71.23057	-18.17019	1
40	-1.792861	5.820057	54.03262	-11.13046	0.9999996
35	-1.331349	4.762261	40.06538	-6.722603	1
30	-0.9546855	3.876614	28.70239	-3.907861	1
25	-0.6503796	3.104254	19.53851	-2.125546	1
20	-0.4100904	2.408997	12.30997	-1.037885	1
15	-0.2281224	1.766689	6.846631	-0.4227766	1
10	-0.1006073	1.159778	3.022516	-0.1222796	0.9999999
-10	-0.1006073	1.159778	3.022516	0.1222796	0.9999999
-15	-0.2281224	1.766689	6.846631	0.4227766	1
-20	-0.4100904	2.408997	12.30997	1.037885	1
-25	-0.6503796	3.104254	19.53851	2.125546	1
-30	-0.9546855	3.876614	28.70239	3.907861	1
-35	-1.331349	4.762261	40.06538	6.722603	1
-40	-1.792861	5.820057	54.03262	11.13046	0.9999996
-45	-2.358851	7.155109	71.23057	18.17019	1
-50	-3.062871	8.984894	92.77639	30.09065	0.9999996

Table 3.13 Results of 500cm radius, 100cm aperture diameter oblate ellipsoid mirror of ε=80.

Y(cm)	**z**(cm)	**Angle**(^{o})	**LA**(cm)	**TA**(cm)	$L^2+M^2+N^2$
50	-3.454915	12.60439	140.3319	-66.06139	0.9999999
45	-2.541901	8.625732	102.5475	-31.84461	0.9999998
40	-1.883938	6.533	75.76304	-17.58352	1.000001
35	-1.376603	5.129882	55.25905	-10.00207	0.9999998
30	-0.9762443	4.067268	39.13975	-5.594545	1
25	-0.65983	3.199594	26.43162	-2.964467	1
20	-0.4136913	2.452799	16.56389	-1.421511	0.9999999
15	-0.2292027	1.783777	9.178543	-0.5718549	0.9999998
10	-0.1008131	1.164493	4.022921	-0.1640472	1
-10	-0.1008131	1.164493	4.022921	0.1640472	1
-15	-0.2292027	1.783777	9.178543	0.5718549	0.9999998
-20	-0.4136913	2.452799	16.56389	1.421511	0.9999999
-25	-0.65983	3.199594	26.43162	2.964467	1
-30	-0.9762443	4.067268	39.13975	5.594545	1
-35	-1.376603	5.129882	55.25905	10.00207	0.9999998
-40	-1.883938	6.533	75.76304	17.58352	1.000001
-45	-2.541901	8.625732	102.5475	31.84461	0.9999998
-50	-3.454915	12.60439	140.3319	66.06139	0.9999999

Tables from 3.14 to 3.17 (for hyperboloids); show a different story to that for all mirrors having $\varepsilon>0$. For the set of ε = {-0.01, -1, -10, -100, -1000} there is a set of Δ = {-2.499938, -2.493781, -2.440442, -2.071068, -1.158312}cm, and for the same interval of asphericity factor the angles' set={5.710314 ^{o}, 5.682445 ^{o}, 5.446473 ^{o}, 4.04472 ^{o}, 1.72703 ^{o}}when the ray height y=50cm. So, it is clear that negatively increase in ε leads to decrease both Δ-values and the angle the incident ray makes with normal. And, as consequent, there is increase in aberrations (TA and LA) over those of spherical mirror of the same paraxial curvature as ε decreases. For the same set of ε above the sets of TA and LA are, respectively, {2.533558E-3, 0.2518625, 2.359148, 14.76136, 34.98063}cm and{-1.235819E-2, -1.252814, -12.25906, -103.8542, -579.5505}cm. The signs of TA and LA refer that the power of the mirror decreased with decreasing ε. So, it is concluded that, the ray above the optical axis intersected the focal plane above the optical axis and vise versa. And that's why the LA has negative values, since all rays intersect the optical axis after the paraxial focal length.

Table 3.14 Results of 500cm radius, 100cm aperture diameter hyperboloid mirror of ε=-0. 01.

y(cm)	z(cm)	Angle(^{o})	LA(cm)	TA(cm)	$L^2+M^2+N^2$
50	-2.499938	5.710314	-1.235819e-2	2.533558e-3	0.9999999
45	-2.024959	5.142585	-8.815289e-3	1.842362e-3	0.9999997
40	-1.599974	4.57376	-8.894682e-3	1.292719e-3	1
35	-1.224985	4.004088	-5.334735e-3	8.63673e-4	0.9999999
30	-0.8999919	3.433591	-2.912462e-3	5.426802e-4	0.9999998
25	-0.6249961	2.862386	-1.70505e-3	3.125207e-4	0.9999999
20	-0.3999984	2.290551	-6.458968e-3	1.602463e-4	1
15	-0.2249995	1.718397	-5.69813e-3	6.777774e-5	0.9999998
10	-0.0999999	1.145688	-1.632071e-2	2.007022e-5	1
-10	-0.0999999	1.145688	-1.632071e-2	-2.007022e-5	1
-15	-0.2249995	1.718397	-5.69813e-3	- 6.777774e-5	0.9999998
-20	-0.3999984	2.290551	-6.458968e-3	-1.602463e-4	1
-25	-0.6249961	2.862386	-1.70505e-3	-3.125207e-4	0.9999999
-30	-0.8999919	3.433591	-2.912462e-3	-5.426802e-4	0.9999998
-35	-1.224985	4.004088	-5.334735e-3	-8.63673e-4	0.9999999
-40	-1.599974	4.57376	-8.894682e-3	-1.292719e-3	1
-45	-2.024959	5.142585	-8.815289e-3	-1.842362e-3	0.9999997
-50	-2.499938	5.710314	-1.235819e-2	-2.533558e-3	0.9999999

Table 3.15 Results of 500cm radius, 100cm aperture diameter hyperboloid mirror of ε=-1.0 .

y(cm)	z(cm)	Angle(^{o})	LA(cm)	TA(cm)	$L^2+M^2+N^2$
50	-2.493781	5.682445	-1.252814	0.2518625	0.9999999
45	-2.020916	5.122199	-1.01321	0.1833478	0.9999996
40	-1.597448	4.55939	-0.8027095	0.1286117	1
35	-1.223503	3.994442	-0.6125259	8.606552e-2	0.9999999
30	-0.8991915	3.427484	-0.4502016	5.414477e-2	0.9999999
25	-0.6246099	2.858759	-0.3198003	3.131366e-2	1.000001
20	-0.3998401	2.288756	-0.2028797	1.601995e-2	1
15	-0.2249494	1.717486	-0.1270948	6.756505e-3	1
10	-0.09999	1.145688	-0.0163108	1.999526e-3	0.9999995
-10	-0.09999	1.145688	-0.0163108	-1.999526e-3	0.9999995
-15	-0.2249494	1.717486	-0.1270948	-6.756505e-3	1
-20	-0.3998401	2.288756	-0.2028797	-1.601995e-2	1
-25	-0.6246099	2.858759	-0.3198003	-3.131366e-2	1.000001
-30	-0.8991915	3.427484	-0.4502016	-5.414477e-2	0.9999999
-35	-1.223503	3.994442	-0.6125259	-8.606552e-2	0.9999999
-40	-1.597448	4.55939	-0.8027095	-0.1286117	1
-45	-2.020916	5.122199	-1.01321	-0.1833478	0.9999996
-50	-2.493781	5.682445	-1.252814	-0.2518625	0.9999999

Table 3.16 Results of 500cm radius, 100cm aperture diameter hyperboloid mirror of ε=-10 .

y(cm)	z(cm)	Angle(°)	LA(cm)	TA(cm)	$L^2+M^2+N^2$
50	-2.440442	5.446473	-12.25906	2.359148	1
45	-1.985575	4.94728	-9.968561	1.738363	1.000001
40	-1.575188	4.434779	-7.900764	1.232813	1
35	-1.210351	3.909811	-6.067437	0.8330724	1
30	-0.8920426	3.373594	-4.467406	0.5286022	0.9999999
25	-0.6211419	2.827293	-3.113696	0.3078906	1
20	-0.3984127	2.272536	-1.99198	0.1584802	0.9999999
15	-0.224496	1.710636	-1.129769	6.713851e-2	1
10	-0.0999002	1.143637	-0.4649667	1.995033e-2	0.9999995
-10	-0.0999002	1.143637	-0.4649667	-1.995033e-2	0.9999995
-15	-0.224496	1.710636	-1.129769	-6.713851e-2	1
-20	-0.3984127	2.272536	-1.99198	-0.1584802	0.9999999
-25	-0.6211419	2.827293	-3.113696	-0.3078906	1
-30	-0.8920426	3.373594	-4.467406	-0.5286022	0.9999999
-35	-1.210351	3.909811	-6.067437	-0.8330724	1
-40	-1.575188	4.434779	-7.900764	-1.232813	1
-45	-1.985575	4.94728	-9.968561	-1.738363	1.000001
-50	-2.440442	5.446473	-12.25906	-2.359148	1

Table 3.17 Results of 500cm radius, 100cm aperture diameter hyperboloid mirror of ε=-100.

y(cm)	z(cm)	Angle(°)	LA(cm)	TA(cm)	$L^2+M^2+N^2$
50	-2.071068	4.04472	-103.8542	14.76136	0.9999997
45	-1.726812	3.827201	-86.56066	11.63348	0.9999998
40	-1.403124	3.57462	-70.30765	8.818869	0.9999998
35	-1.103278	3.282112	-55.26275	6.359231	0.9999999
30	-0.8309519	2.945236	-41.60782	4.29267	1
25	-0.59017	2.560632	-29.54044	2.647403	1
20	-0.3851648	2.126884	-19.27834	1.433467	1
15	-0.2201533	1.645919	-11.01396	0.6333959	1
10	-9.901951E-2	1.123439	-4.970037	0.194307	1
-10	-9.901951E-2	1.123439	-4.970037	- 0.194307	1
-15	-0.2201533	1.645919	-11.01396	-0.6333959	1
-20	-0.3851648	2.126884	-19.27834	-1.433467	1
-25	-0.59017	2.560632	-29.54044	-2.-647403	1
-30	-0.8309519	2.945236	-41.60782	-4.29267	1
-35	-1.103278	3.282112	-55.26275	-6.359231	0.9999999
-40	-1.403124	3.57462	-70.30765	-8.818869	0.9999998
-45	-1.726812	3.827201	-86.56066	-11.63348	0.9999998
-50	-2.071068	4.04472	-103.8542	-14.76136	0.9999997

After discussing the previous tables, one thing should be cleared; the previous tables included column entitled "$L^2+M^2+N^2$". This column gives the validity of the skew ray tracing condition pointed out in equation 2.14 of **§2.2.** Those columns, often, show the $L^2+M^2+N^2 \approx 1$, this can be ascribed to the very well-known machine intrinsic numerical errors, specifically, truncation (cut-off) error and rounding-off error.

Summary

It is, somewhat, necessary to summarize the previous discussion before going to the next section. Table 3.18 gives a brief comparison and summarizes the discussion of the tables form 3.4 to 3.17 ,since it shows the variation in the values of angle the incident ray (marginal or semi-aperture ray, when y=50cm)makes, and the corresponding Δ, LA, and TA. This table, also, shows the Δ-values in region near to the paraxial one, when y=10cm.

Table 3.18 Results of 500cm radius, 100cm aperture conic surfaces.

		y=50cm				y=10cm
Asphericity factor (ε)	ε	**Δ(cm)**	**Angle(^{o})**	**LA (cm)**	**TA (cm)**	**Δ (cm)**
Oblate ellipsoid	80	-3.454915	12.60439	140.3319	-66.06139	-0.1008131
	60	-3.062871	8.984894	92.77639	-30.09065	-0.1006073
	40	-2.817542	7.356153	56.76044	-14.90397	-0.1004032
	20	-2.63932	6.379349	26.54819	-6.011672	-0.1002008
Sphere	1	-2.506281	5.739176	1.259664	-0.2557378	-0.10001
Prolate ellipsoid	0.8	-2.50502	5.733401	1.00618	-0.2042748	-0.100008
	0.6	-2.503761	5.727655	0.7534409	-0.1529703	-0.100006
	0.4	-2.502505	5.721972	0.5029576	-0.1018295	-0.100004
	0.2	-2.501251	5.716318	0.2532806	-5.084326e-2	-0.100002
Parabo-Loid	0	-2.5	5.710623	0	5.164608e-6	-0.1
hyper-boloid	-0.01	-2.499938	5.710314	-1.235819e-2	2.533558e-3	-0.0999999
	-1	-2.493781	5.682445	-1.252814	0.2518625	-0.09999
	-10	-2.440442	5.446473	-12.25906	2.359148	-0.0999002
	-100	-2.071068	4.04472	-103.8542	14.76136	-9.901951e-2
	-1000	-1.158312	1.727031	-579.5505	34.98063	-9.160798e-2

It is clear that increasing ε leads to increase Δ and LA, and TA (with negative sign) referring to the increase in the power of the mirror surface that made the reflected ray intersect the optical axis before the focal point and then intersects the focal image plane below the optical axis. All this is ascribed to the increase in the angle the incident rays make with surface normal. Surfaces with $\varepsilon>0$ represent this behavior (prolate ellipsoids, spherical surfaces, and oblate ellipsoids).

In the case of hyperboloids the situation is the contrast. TA in this case possesses positive vales while LA possesses negative values because the reflected rays intersect the focal image plane above the optical axis and then intersect the optical axis behind the focal point due to the decrease in the angle the reflected rays made with the surface.

This table shows the case of paraboloid as the interface between the region of positive LA, and negative TA to negative LA, and positive TA.

Δ-values when y=50cm varies from1.158cm to 3.454cm, when ε varies form -1000 to 80. And when y=10cm(R.H.S column), the region near to the paraxial one, Δ- values varies from 9.160798E-2cm to 0.1008131cm for the same interval of ε. These infinitesimal variation in Δ- values refers that they are slightly affect by ε and at the same time exhibit the dominance of the paraxial curvature.

3.3 Conclusions

1. The asphericity factor changes the shape of conic surfaces and consequently changes the telescope mirrors parameters of this thesis (the TA, LA, and the Δ-values);
2. ε varies the distance between the conic surfaces and the tangent plane at the edge of the surface for D =1m is in the range of μm for the interval [ε<1]. i.e., all conics except the oblate elliposoid; while the distance between the surfaces and the tangent plane at the edge of the surface is in the range of mm (ε>1). This is shown by Δ-values column for the marginal ray (semi-aperture ray, y=50cm) in table 3.18. and that's why the domain of aperture diameter of oblate ellipsoid is [-50, 50]cm, and that for others is[-500, 500]cm;
3. more negatively values of ε (hyperboloids) produces more flattened surfaces, and when ε goes to $-\infty$ the surface becomes plane;
4. in the interval ε > 1, the angles incident rays make with the vector normal to the surface are getting bigger, and in the interval ε < 0 the angles become smaller and smaller; thus when ε goes to $-\infty$ the angle becomes zero, i.e. the incident ray completely coincides the vector normal to the surface;
5. increasing ε increases the power of the surface leading to negatively TA values and vise versa;
6. when ε>0 the power of the surface beyond the paraxial region is larger than that for the paraxial one, and when ε<0 the power of the surface beyond the paraxial region is lower than that for the paraxial one;
7. according to figures 3.1, 3.2, 3.3, and 3.4 and the corresponding tables (3.1, 3.2, 3.3), it is concluded that when the aperture diameter D≤ R/10, the of paraxial curvature (c=1/R) is the dominant factor in shaping the conic surfaces, since the change in Δ-values (departure from the spherical surface) is in the rang of μm; beyond this region (D≤

R/10) the influence of ε increases dramatically in shaping the conic (Cartesian) surfaces and the Δ-values increases from millimeters to centimeters; and this in turn has, of course, its reflection on the power of the surface;

8. According to the performance surfaces showed, the paraboloid should be considered to stand for the telescope primary mirror; because of its excellent performance.

Chapter 4

The Basic Design of Reflecting Telescope

This chapter explains the design steps and the considered procedures to determine and to choose the optimum secondary mirror radius. This procedure based upon the Extreme-Value Theorem; therefore this chapter introduces it in short. Also, it exhibits the characteristics and the features of the complete system**.** The following section gives the priority of design steps in a descending manner.

4.1 Design Steps

1. The telescope configuration

   The chosen configuration of mirrors arrangement is that of Cassegrian because it is symmetrical about the axis of revolution (easier to control aberrations in such systems) and shortest among other configurations.

2. the choice of paraboloid, with R1=-5m and apertuere diameter $D1$=1m, as primary mirror is for two goals:

   first, eliminating spherical aberrations, and second improving the resolving power.

3. On the light of light gathering power importance, minimum light obstruction should be taken into account. The distance of separation (d) between the two mirror is the key for this point. So, for 0.25% obstruction (light obstruction) from the area of the primary, the secondary aperture diameter shouldn't exceed 5cm.

This means that the height of the semi-aperture ray(marginal ray, y=50) at the secondary mirror is ≤ 2.5cm. To obtain this light obstruction the distance separating (*d*) the two mirrors, equation $y_0 = y_{-1} + \frac{M}{N}(d - z_{-1})$ has been employed by applying the skew ray tracing code through the primary mirror (paraboloid) and the yielded *d* is=237.625cm, so the considered separating distance between the two mirrors is *d*=238cm.

4. The system focal plane:

   The key for this point is the selection of radius of curvature (R2). The proper determination of R2 is restricted by the value of aberration yielded.

4.2 The Extreme-Value Theorem

The Extreme-Value Theorem (very well-known in Calculus) is the one for solving optimization problems. It helps to find out the point that verifies the local maximum or local minimum of a certain function; and the local minimum, of course, is the point of search to stands for R2 while TA stands for the function. The point of local minimum (or maximum) is very special one; because at this point the function behavior witnesses a change. This change is either form positive function values to the negative or from decreasing to increasing or vice versa; Figure 4.1 shows this meaning

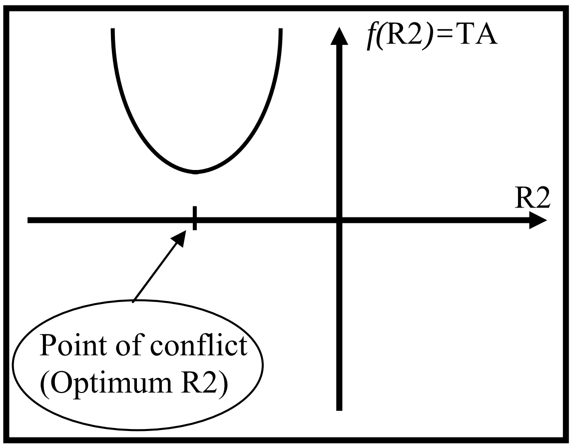

Figure 4.1 Extreme-Value Theorem.

4.3 Optimum Secondary Mirror Radius Determination

The selection of the proper R2 is of great importance; because it is the dominant factor as explained in the §3.2 and §3.3. Thus, designer should consider the radius of curvature as the master key to reduce mirrors aberration besides being the unique parameter that defines the system focal length. Determining R2 has achieved by applying the skew ray tracing code through the primary and the secondary mirrors taking into account the telescope configuration and characteristics determined in §.4.1. The procedure used for R2 determination is based upon the Extreme-Value Theorem. The procedure steps are:

1. since the considered system configuration is that for Cassegrian, hence, R2 has a negative sign
2. initially, the secondary mirror surface has considered as spherical surface. In this part, the search of the proper R2 is based upon observing the performance of the surface that has certain value of R2 and resuming in the direction that shows aberration reduction at the image focal plane.
3. the procedure of the previouspoint goes on until the performance witnesses a behavior change. The point of behavior change is the proper R2.

Table 4.1 shows the ray tracing results through the telescope system, where y1 is the height of ray incident on the primary mirror (M1), y2 is the height of the ray reflected from M1 at the secondary mirror (M2), y(x-y)plane is the height of ray reflected from M1 at the (x-y) plane that is tangent to M2, angle1 and angle2 are the angles the incident ray makes with the normal vectors at the points of incidence at M1 and M2 respectively, and finally, TA is used as the performance meter. According to table 4.1 the proper R2=-25cm; because before this point (value) at R2=-26cm, TA values were < 0, and after this point (at R2=-24cm), TA values were>0 and greater than those for R2=-25cm.

4. although R2 at -25cm represents the confliction point but the yielded TA-values (0.0402654cm and 0.6576515cm) are quite not satisfying. To improve the performance (reducing TA) of M2, point No.2 should be repeated but between R2=-25cm and the neighbor R2 value that gives least differences in TA values, i.e. between R2= -25 cm and R2=-26cm. Then, the new point of confliction in the performance is the optimum R2 value.

Table 4.2 shows that R2=-25.21cm is the point of confliction, which is the optimum desired radius of curvature that gives TA= 2.832694e-4cm or 2832.694nm when yM1=5cm (in the region near the paraxial). Since, the wavelength average value of light (visible region) λ=550nm, hence, TA ≈5λ. Optical systems possessing aberrations in the range of only multiple number of wavelength, its performance is considered as excellent and this is the goal of optical design. But, at the edge (yM1=50cm) there is a considerable amount of TA= 0.2596356cm.

Table 4.1 Proper R2 Determination

R2 (cm)	y1(cm)	Angle1(^{o})	y(x-y)plane (cm)	Y2(cm)	Angle2(^{o})	TA(cm)
-26	5	0.5726662	0.2400243	0.2400021	0.6161205	-0.144342
	50	5.710623	2.424235	2.401776	6.120997	-1.180455
-25	5	0.5726662	0.2400243	0.2400021	0.5947903	0.0402654
	50	5.710623	2.424235	2.400891	5.91039	0.6576515
-24	5	0.5726662	0.2400243	0.2400003	.5719823	0.2402559
	50	5.710623	2.424235	2.399933	5.682307	2.648018

Table 4.2 Optimum R2 Determination

R2 (cm)	y(cm)	Angle(^{o})	y(x-y)plane (cm)	Y2(cm)	Angle(^{o})	TA(cm)
-25.20	5	0.5726662	0.2400243	.2400014	0.5990518	2.171709e-3
	50	5.710623	2.424235	2.401073	5.953843	0.2784324
-25.21	5	0.5726662	0.2400243	0.2400243	0.5993783	2.832694e-4
	50	5.710623	2.424235	2.401082	5.955982	0.2596356
-25.22	5	0.5726662	0.2400243	0.2400014	0.5997047	-1.603802e-3
	50	5.710623	2.424235	2.401091	5.958154	0.2408468

5. the value of TA yielded at the mirror edge of M2 and the region beyond the paraxial can be moderated (reduced) by varying ε of M2, i.e. adapting quadratic or Cartesian surface rather than spherical, to obtain the maximum acceptable aberrations.
6. according to §3.3 (referring to point 5 and 6 specifically), to moderate aberration away from the paraxial region the needed surfaces to stand for M2 are those of $\varepsilon < 0$, i.e. hyperboloids.

Table 4.3 shows that ε=-0.21 is the required value that gives the minimum possible aberrations; where TA= 225.2726nm <λ/2, and 3924.088nm (≈7 folds of λ) when yM1=5cm and 50cm respectively. The basic concept for this choice is also the point of confliction considered before to obtain the proper and optimum R2.

Table 4.3 Asphericity factor (ε) Determination of R2

ε2	yM1(cm)	Angle(^{o})	y(x-y)plane (cm)	yM2(cm)	Angle(^{o})	TA(cm)
-0.20	5	0.5726662	0.2400243	0.2400014	0.5993783	2.485558e-5
	50	5.710623	2.424235	2.401144	5.985365	2.510515e-3
-0.21	5	0.5726662	0.2400243	0.2400014	0.5993783	2.252726e-5
	50	5.710623	2.424235	2.401145	5.985662	3.924088e-4
-0.22	5	0.5726662	0.2400243	0.2400014	0.5997047	1.985069e-5
	50	5.710623	2.424235	2.401145	5.985956	-1.74245e-3

4.4 Telescope Characteristics

- Telescope configuration: Cassegrian.
- M1 central cavity of 5cm diameter.

Table 4.4 Telescope Characteristics

	R (cm)	*D (cm)*	*ε*	*Distance (cm)*	*position*
M1	-500	100	0		
M2	-25.21	5	-0.21		
d1				-238	to the left of M1
d2				250	12 cm to the right of M1

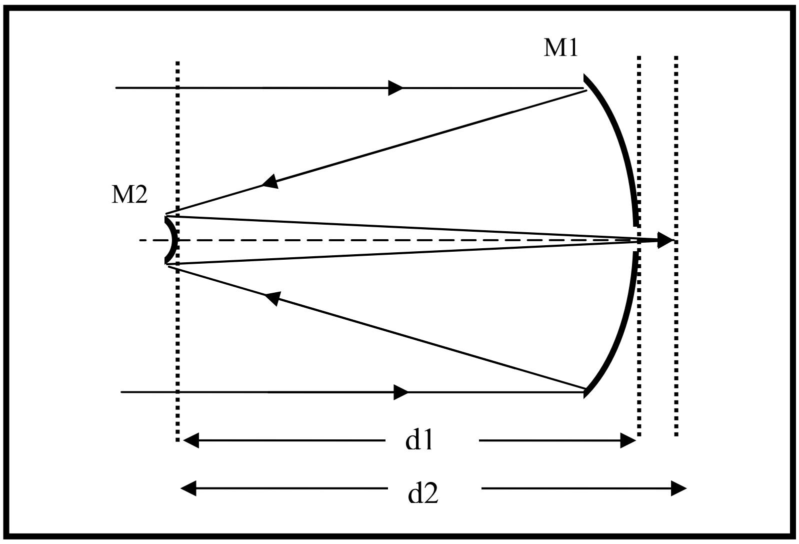

Figure 3.5 The Telescope Configuration.

4.5 Telescope Features

Telescope features, this term refers to the telescope three powers.

1. according to equation1.1

   the telescope magnification power $\frac{250cm}{0.5cm}$ = 500 X, where 0.5cm is

   the focal length of the assumed eye-piece.

2. according to equation 1.4 :

   the linear separation = $1.22\frac{\lambda}{n\sin(U)} = \frac{550nm}{n\sin(2\times 5.710623)} = 3.388\mu m$

where, U is the convergence angle=2$\times$angle of reflection, while according to equation 1.2 (for spherical surfaces) the linear separation= $1.22\dfrac{\lambda}{D}f = 1.22\dfrac{550nm}{1m}\times 2.5m = 1.677\,\mu m$

3. Central light obstruction $=[\dfrac{D2^2}{D1^2}=\dfrac{5^2}{100^2}=\dfrac{25}{10000}]\times 100\%$ =0.25%

4.6 Conclusions

1. the procedure used in aberration reduction (finding out the point of behavior change) showed acceptable results in aberrations reduction. It may be, also, able to eliminate, completely, spherical aberration if the distance (*d*) separating the two mirrors would be involved in the optimization procedure.
2. the paraboloid mirror showed improvement in resolution over that of spherical surfaces, so increasing the primary depth of paraboloid, in other words the aperture, would increase the resolution over the resolution spherical surfaces, of the same aperture, give.
3. the design improved the light gathering power of 1m aperture telescope for light obstruction =0.25% (less than 1%).

4.7 Future Work

1. Designing a system corrected for both spherical and coma, where both mirrors are hyperboloids;
2. Considering the Strehel ratio as principal point for system aberration reduction;
3. Considering the wavefront aberration or the optical transfer function as a measure for exhibiting the system performance.

Appendix

Derivation of Δ in Spherical Surfaces

$$z = \frac{c}{2}\left(x^2 + y^2 + z^2\right) \qquad (2.1)$$

$$\left.\begin{aligned} x &= x_o + L\Delta \\ y &= y_o + M\Delta \\ z &= N\Delta \end{aligned}\right\} \qquad (2.5)$$

Substituting (2.5) in (2.1) yields

$$N\Delta = \frac{c}{2}\left[(x_o + L\Delta)^2 + (y_o + M\Delta)^2 + (N\Delta)^2\right]$$

$$N\Delta = \frac{c}{2}\left[x_o^2 + 2x_oL\Delta + L^2\Delta^2 + y_o^2 + 2y_oM\Delta + M^2\Delta^2 + N^2\Delta^2\right]$$

$$N\Delta = \frac{1}{2}c\left(x_o^2 + y_o^2\right) + \frac{2}{2}c\left(Lx_o + My_o\right)\Delta + \frac{c}{2}\Delta^2\left(L^2 + M^2 + N^2\right)$$

Since $L^2 + M^2 + N^2 = 1$, and $F = c\left(x_o^2 + y_o^2\right)$

Then the later equation in terms of equations (2.7) and (2.14) is:

$$N\Delta = \frac{F}{2} + c\left(Lx_o + My_o\right)\Delta + \frac{c}{2}\Delta^2$$

$$0 = \frac{F}{2} - \left[N - c\left(Lx_o + My_o\right)\right]\Delta + \frac{c}{2}\Delta^2$$

Now the later equation in terms of the equation $G = N - c\left(Lx_o + My_o\right)$ (2.8)

becomes:

$$\frac{c}{2}\Delta^2 - G\Delta + \frac{F}{2} = 0$$

which is similar to $ax^2 + bx + c = 0$ that is solved by

$$x = \frac{-b \pm \sqrt{b^2 - 4ac}}{2a}$$

$$\therefore \quad 2ax = -b \pm \sqrt{b^2 - 4ac}$$

$$\therefore \quad a = \frac{c}{2} \quad , \quad b = -G \quad , \quad c = \frac{F}{2}$$

$$\therefore \quad c\Delta = G \pm \sqrt{G^2 - cF}$$

Now by multiplying the R.H.S of equation of the later equation with the negative sign by the quantity $\left(G + \sqrt{G^2 - cF}\right)$ and dividing the result by the same quantity $\left(G + \sqrt{G^2 - cF}\right)$ yields

$$\Delta = \frac{F}{G + \sqrt{G^2 - cF}}$$, which it is equation (2.6)

Derivation of Δ in Quadric Surfaces of Revolution

$$z = \frac{c}{2}\left(x^2 + y^2 + \varepsilon z^2\right) \tag{2.15}$$

$$\left.\begin{aligned} x &= x_o + L\Delta \\ y &= y_o + M\Delta \\ z &= N\Delta \end{aligned}\right\} \tag{2.5}$$

Appling (2.5) in (2.15) yields

$$N\Delta = \frac{c}{2}\left[(x_o + L\Delta)^2 + (y_o + M\Delta)^2 + \varepsilon N^2\Delta^2\right]$$

$$N\Delta = \frac{c}{2}\left[x_o^2 + 2Lx_o\Delta + L^2\Delta^2 + y^2 + 2My_0\Delta + M^2\Delta^2 + \varepsilon N^2\Delta^2\right]$$

$$N\Delta = \frac{c}{2}\left[\left(x_o^2 + y_o^2\right) + 2\left(Lx_o + My_o\right)\Delta + L^2\Delta^2 + M^2\Delta^2 + \varepsilon N^2\Delta^2\right]$$

$$N\Delta = \frac{c}{2}\left(x_o^2 + y_o^2\right) + c\left(Lx_o + My_o\right)\Delta + \frac{c}{2}\Delta^2\left(L^2 + M^2 + \varepsilon N^2\right)$$

$$c\Delta^2 .\frac{1}{2}\left(L^2 + M^2 + \varepsilon N^2\right) - \left[N - c\left(Lx_o + My_o\right)\right]\Delta + \frac{c}{2}\left(x_o^2 + y_o^2\right) = 0$$

since $F = c\left(x_o^2 + y_o^2\right)$; *and* $G = N - c\left(Lx_o + My_o\right)$

hence, the later equation becomes:

$$\frac{c}{2}.\left(L^2 + M^2 + \varepsilon N^2\right)\Delta^2 - G\Delta + \frac{F}{2} = 0$$

Since $L^2 + M^2 + N^2 = 1$ hence, $L^2 + M^2 = 1 - N^2$

Now the equation before later expression becomes:

$$\frac{c}{2}\left(1 - N^2 + \varepsilon N^2\right)\Delta^2 - G\Delta + \frac{F}{2} = 0$$

$$\frac{c}{2}\left[1 + (\varepsilon - 1)N^2\right]\Delta^2 - G\Delta + \frac{F}{2} = 0$$

To solve for Δ using $x = \dfrac{-b \pm \sqrt{b^2 - 4ac}}{2a}$

To solve $ax^2 + bx + c = 0$, it's found that

$\frac{c}{2}\left[1 + (\varepsilon - 1)N^2\right] = a$, G=b, and $\frac{F}{2} = c$

$$c\Delta = \frac{G \pm \sqrt{G^2 - 4 * \frac{c}{2}\left[1 + (\varepsilon - 1)N^2\right] * \frac{F}{2}}}{\left[1 + (\varepsilon - 1)N^2\right]}$$

$$c\Delta = \frac{G \pm \sqrt{G^2 - cF(1 + (\varepsilon - 1)N^2}}{\left[1 + (\varepsilon - 1)N^2\right]}$$

By the same manner used to obtain Δ in spherical surfaces

$$\Delta = \frac{G - \sqrt{G^2 - cF(1 + (\varepsilon - 1)N^2}}{\left[1 + (\varepsilon - 1)N^2\right]} \bullet \frac{G + \sqrt{G^2 - cF(1 + (\varepsilon - 1)N^2}}{G + \sqrt{G^2 - cF(1 + (\varepsilon - 1)N^2}}$$

$$\Delta = \frac{F}{G + \sqrt{G^2 - cF(1 + (\varepsilon - 1)N^2}}$$ which is equation (2.16)

Derivation of the Direction Cosines of the Surface Normal Vector

Now, to find the cosine of the incident angle ray makes by applying

$$\alpha, \beta, \gamma = \frac{-[(\frac{\partial F}{\partial x}, \frac{\partial F}{\partial y}, \frac{\partial F}{\partial z})]}{\sqrt{(\frac{\partial F}{\partial x})^2 + (\frac{\partial F}{\partial y})^2 + (\frac{\partial F}{\partial z})^2}} \qquad (1)$$

To the equation of quadric surface $z = \frac{c}{2}(x^2 + y^2 + \varepsilon z^2)$ (2.15)

1. rewriting the later in the form of $F = x^2 + y^2 + \varepsilon z^2 - 2rz = 0$ (2)

Where r=1/c and equation (2) is $cx^2 + cy^2 + c\varepsilon z^2 - 2z = 0$ (3)

2. differentiating equation (2) yields

$$\frac{\partial F}{\partial x} = -2cx \ , \quad \frac{\partial F}{\partial y} = -2cy, \quad \frac{\partial F}{\partial z} = 2c\varepsilon z - 2 \qquad (4)$$

$$(\frac{\partial F}{\partial x})^2 = 4c^2x^2, \quad (\frac{\partial F}{\partial y})^2 = 4c^2y^2, \quad (\frac{\partial F}{\partial z})^2 = 4c^2\varepsilon^2z^2 - 8c\varepsilon z + 4$$

$$(\frac{\partial F}{\partial x})^2 + (\frac{\partial F}{\partial y})^2 = 4c^2(x^2 + y^2) \qquad (5)$$

But according to (3) $c = (x^2 + y^2) = 2z - c\varepsilon z$

$$\therefore \sqrt{(\frac{\partial F}{\partial x})^2 + (\frac{\partial F}{\partial y})^2 + (\frac{\partial F}{\partial z})^2} = \sqrt{4c(2z - c\varepsilon z^2) + 4c^2\varepsilon^2 z^2 - 8c\varepsilon z + 4}$$

$$= 2\sqrt{2cz - -c^2\varepsilon z^2 + c^2\varepsilon^2 z^2 - 2c\varepsilon z + 1}$$

$$= 2\sqrt{1 + 2c(1-\varepsilon)z + c^2(\varepsilon - 1)\varepsilon z^2}$$

$$= 2\sqrt{1 - 2c(\varepsilon - 1)z + c^2\varepsilon(\varepsilon - 1)z^2} \qquad (6)$$

Substituting (6) and (4) in (1) yields

$$\alpha, \beta, \gamma = \frac{-[2cx, 2cy, 2c\varepsilon z - 2]}{2\sqrt{1 - 2c(\varepsilon - 1)z + c^2\varepsilon(\varepsilon - 1)z^2}}$$

$$\alpha,\ \beta,\ \gamma = \frac{-cx, -cy, 1 - c\varepsilon z}{\sqrt{1 - 2c(\varepsilon - 1)z + c^2\varepsilon(\varepsilon - 1)z^2}}$$ and the final is equation (2.17)

Derivation of the Cosines of the incident Angle

$$\cos I = (Li + Mj + Nk) \bullet (\alpha i + \beta j + \gamma k)$$

$$= Li \bullet \alpha i + Mj \bullet \beta j + Nk \bullet \gamma k$$

$$= L \bullet \frac{-cx}{\sqrt{1 - 2c(\varepsilon - 1)z + c^2\varepsilon(\varepsilon - 1)z^2}} + M \bullet \frac{-cy}{\sqrt{1 - 2c(\varepsilon - 1)z + c^2\varepsilon(\varepsilon - 1)z^2}} +$$
$$N \bullet \frac{1 - c\varepsilon z}{\sqrt{1 - 2c(\varepsilon - 1)z + c^2\varepsilon(\varepsilon - 1)z^2}}$$

$$\cos I = \frac{-Lcx - Mcy + N(1 - c\varepsilon z)}{\sqrt{1 - 2c(\varepsilon - 1)z + c^2\varepsilon(\varepsilon - 1)z^2}}$$

$$\cos I = \frac{N - c(Lx + My1 + N\varepsilon z)}{\sqrt{1 - 2c(\varepsilon - 1)z + c^2\varepsilon(\varepsilon - 1)z^2}}$$

which is equation 2.18.

References

[1] D. Baker
The Hamlyn Guide to Astronomy
The Hamlyn Publishing Group (1978)

[2] Alexander Goncharov
Extremely Large Telescopes Optical Design and Wavefront Correction
Ph. D. Thesis (Lund Observatory/ Lund Universitet 2003)

[3] R.Guenther
Modern Optics
John Wiley & Sons (1990)

[4] Cost Effective Mirror fabrication
Section 5.4 of the 'GMST Handbook', N10-RMT-0006
Also posted on: http://www.aura-nio.noao.edu/book/ch5/5_1.html

[5] F. G. Smith and J. H. Thomson
Optics, "2nd. Edition".
John Wiley & Sons (1988)

[6] C. S. William and O. A. Becklund
Optics: A Short Course for Engineers & Scientists
John Wiley & Sons (1972)

[7] http://users.zoominternet.net/~matto/M.C.A.S/
ightgathering_power.htm #Light-gathering%20power (Nov.2006)

[8] http://www.thunderbirdtechnology.com/Other%20Pages/
AiryDiscAndAngularResolution.htm (Nov.2006)

[9] http://www.twcac.org/Tutorials/notes(4).htm#Seeing (Nov.2006)

[10] http://users.zoominternet.net/~matto/M.C.A.S/
lightgathering_power.htm#Light-gathering%20power (Nov.2006)

[11] R. S. Longhurst
Geometrical & Physical Optics "3rd. edition"
Longman (1990)

[12] J. M. Palmer
Monographs on Applied Optics (Lens Aberration Data)
Adam Hilger (1971)

[13] D.C. O'Shea
Elements of Modern Optical Design.
John Wiley & Sons (1985)

[14] J. Meyer
Introduction to Classical & Modern Optics, "2nd. edition"
Prentice–Hall (1989)

[15] W. J. Smith
Handbook of Optics (Sponsored by the Optical Society of America)
McGraw- Hill (1978)

[16] W. J. Smith
Modern Optical Engineering (The Design of Optical Systems)
McGraw-Hill (1966)

[17] C.S. Williams & O. A. Becklund
Introduction to Optical Transfer Function.
John Wiley & Sons (1989)

[18] M. Born & E. Wolf
The Principles of Optics, "5th.edition"
Pergamon Press (1975).

[19] W. T. Welford
Aberrations of the Symmetrical Optical System.
Academic Press (1974)

[1]† Mountain M.
What is beyond the current generation of ground-based 8-m to 10-m class telescopes and LT-I?
Proc. SPIE. 2871, 597-606, 1996.

[2]† Benn C.R. and Ellison S.L.
Brightness of the night sky over La Palma
New Astronomy Reviews 42, 503-507, 1998.

[3]† Roggemann M.C., Welssh B.M., and Rugate R.Q.
Improving the resolution of ground-based telescopes
Rev. Mod. Phys. 69, 437-505, 1997.

[4]† Hardy J.W., Active optics
A new technology for the control of light
Proc. IEEE 66, 651–697, 1978.

[5]† Hardy J.W.
Adaptive optics – a progress review
Proc. SPIE 1542, 2-17, 1991.

[6]† Beckers J.M.
Adaptive optics for Astronomy: Principles, Performances, and Applications
*Annu. Rev. Astron.Astrophys.*31,13-62, 1993.

[7]† Sasiela, R.J.
Wave-front correction by one or more synthetic beacons
J.Opt.Soc.Am. A 11, 379-93., (1994).

[8]† Schmidt-Kaler T. and Rucks P.
Telescope costs and cost reduction
Proc. SPIE 2871, 635-640, 1996.

[9]† Dekany R., Nelson J., and Bauman B.
Design considerations for CELT adaptive optics
Proc. SPIE 4003, 682-690, 2000.

[10]† Sebring T., Bash F., Ray F., and Ramsey L.
The Extremely Large Telescope: Further Adventures in Feasibility
Proc. SPIE 3352, 792-800, 1998.

[11]† Andersen T., Ardeberg A., Beckers J., Flicker R., Gontcharov A., Jessen N.C., Mannery E. and Owner-Petersen M.
The proposed 50 m Swedish Extremely Large Telescope
Proc. Bäckaskog Workshop onExtremely Large Telescopes, 72-82, 1999.

[12]† Gilmozzi R., Delabre B., Dierickx P., Hunin N., Koch F., Monnet G., Quattri M., Rigaut F., and Wilson R
The future of filled aperture telescopes: is a 100m feasible
Proc. SPIE 3352, 778–791, 1998.

[13]† Enard D.
ESO VLT: status of the main 8-meters telescopes
Proc. SPIE 2199, 394-403, 1994.

[14]† Nelson J. and Gillingham P.
Overview of the performance of the W.M.Keck Observatory
Proc. SPIE 2199, 82-93, 1994.

[15]† Smith G.
Keck II status report
Proc. SPIE 2871, 10-14, 1996.

[16]† Hill J.
The Large Binocular Telescope Project
Proc. SPIE 2871, 57-68, 1996.

[17]† Rodriguez Espinosa J. and Alvarez Martin P.
Gran Telescopio Canarias: A 10 m telescope for the ORM
Proc. SPIE 2871, 69-73, 1996.

[18]† Sebring T.
The Hobby-Eberly telescope: A progress report
Proc. SPIE 2871, 32-37, 1996.

[19]† Kaifu N
Status and perspective of Subaru Telescope Project
Proc. SPIE 2871, 24-29, 1996.

[20]† Mountian M., Gillett F., and Kurz R.
The Gemini 8-M Telescope Project
Proc. SPIE 2871, 15-23, 1996.

[21]† Dierickx P.
Optical fabrication in the large
Proc. Bäckaskog Workshop on Extremely Large Telescopes, 224-236, 1999.

[22]† Karoji H.
Status of Subaru 8.2 Mirror Fabrication
Proc. SPIE 2871, 393-398, 1996.

[23]† Dierickx P. and Enard D.
The VLT primary mirror: mirror production and measured performance
Proc. SPIE 2871, 385-404, 1996.

[24]† Angel R. and Hill J.
Manufacture of large glass honeycomb mirrors
Spec .Pub. SPIE. A83-30976-13-89, 298-306, 1982.

[25]† Stepp L., Huang E., and Cho M.
Gemini primary mirror support system
Proc. SPIE 2199, 223-238, 1994.

[26]† Cho M.
Active optics performance study of the primary mirror of
the Gemini Telescopes Project
Proc. SPIE 2871, 272-290, 1996.

[27]† Gray P., Hill J., Davison W., Callahan S., and Williams J.
Support of large borosilicate honeycomb mirrors
Proc. SPIE 2199, 691-702, 1994.

[28]† Shack R. and Platt B.
Production and use of lenticular Hartmann screen
J. Opt. Soc. Am. 61, 1586 -1590, 1971.

[29]† Cannon R.C.
Global wavefront reconstraction using Shach-Hartmann sensor
J. Opt. Soc. Am. A 12, 2031-2039, 1995.

[30]† Jochum L., Castro J., and Devaney N.
Gran Telescopio Canarias: current status of its optical design and
opto-mechanical support system
Proc. SPIE 3352, 621-626, 1998.

[31]† Beckers J.
Extremely Large Multiple Mirror Telescope
Proc. Bäckaskog Workshop on Extremely Large Telescope, 83-91, 1999.

[32]† Arnold L.
Multiple-Mirror-Telescope concept for a very compact 50m
Extremely Large Telescope
Proc. Bäckaskog Workshop on Extremely Large Telescopes, 92-96, 1999.

[33]† Beckers J., Ulich B., and Williams J.
Performance of the Multiple Mirror Telescope (MMT). I. MMT, the first of advance technology telescopes
Spec. Pub. SPIE. A83-30976-13-89, 2-8, 1982.

[34]† Beckers J., Ker-Li Shu, and Shaklan S.
Planning the National New Technology Telescope (NNTT),
IV The Coalignment, Cophasing
System, *Proc. SPIE* 628, 102-108, 1986.

[35]† Schmidt-Kaler Th.
Coating Technologies
Astron. Nachr. 315, N4, 323. 1994.

[36]† Jacobson M.R., *et al*.
Development of silver coating options for the Gemini 8-M Telescope Project
Proc. SPIE 3352, 477-485, 1998.

[37]† Geyl R. and Cayrel M.
Extremely large telescopes - a manufacturer point of view
Proc. Bäckaskog Workshop on Extremely Large Telescopes, 237-241, 1999.

[38]† West S., *et al.*
Progress at the Vatican Advanced Technology Telescope
Proc. SPIE 2871, 74-85, 1996.

[39]† Barbieri C.
The Galileo Italian National Telescope and its Instrumentation
Proc. SPIE. – 1996. – V.2871. – C. 244–253.

[40]† Korhonen T. and Lappalainen L.
Flexible membrane tools for mirror figuring
Proc. SPIE 1236 ,691-698, 1990.

[41]† Lubliner J. and Nelson J.
Stressed mirror polishing: a technique for producing non-axisimmetric mirrors
Appl. Opt. 19, 2332, 1984.

[42]† Allen L.
Progress in ion figuring large optics
XXVI Boulder Damage Symposium on Optical Materials for High Power Lasers 1994.

[43]† Malacara D.
Optical shop testing
John *Wiley and Sons* , New York 1978.

[44]† Anderson D. and Burge J.
Swing-arm profilometry of aspherics
Proc. SPIE 2536, 1995.

[45]† Puryayev D.T.
Optical test methods for aspheric surfaces
Nauka 1976.

[46]† Wilson R.N.
Reflecting Telescope Optics II
Springer 1999.

[47]† Gildner D. and Carbone F.
Deterministic, Cost-Effective Optical Processing of Spherical and Aspheric Mirror Segments for Extremely Large Telescopes
Proc. Bäckaskog Workshop on Extremely Large Telescopes, 242-248, 1999.

[48]† Burge J.
Measurement of large convex aspheres
Proc. SPIE 2871, 362-373, 1996.

[49]† Coulman C.E.
Fundamental and applied aspects of astronomical ”seeing”
Annu.Rev. Astron.Astrophys. 23,19-57,1985.

[50]† Fried D. L.
Optical resolution through a randomly inhomogeneous medium for very long and very short exposures
J. Opt. Soc. Am. 56, 1380 –1384, 1966.

[51]† Fried D. L.
Anisoplanatism in adaptive optics
J. Opt. Soc. Am. 72, 52 – 61, 1982.

[52]† Kolmogorov A. N.
In *Tuirbulance, Classical papers on Statistical Theory*
151-155, Transl. Friedlander, Topper L., New York,1961.

[53]† Noll R.J.
Zernike polynomials and atmospheric turbulence
J. Opt. Soc. Am. 66, 207–211, 1976.

[54]† Pollaine S., Buffington A., and Crawford F.S.
Measurement of the size of the isoplanatic patch using a phase-correcting telescope
J. Opt. Soc. Am. 69, 84 –89, 1979.

[55]† Aliva R.
Observational methods for the study of optical turbulence
ASP Conference Series, ed. Verinin J., Z.Benkhaldoun,
Muñoz-Tuñón, 266, 48-63, 2002.

[56]† McCLURE R.D., Arnaud J., Fletcher J. M., Nieto J.-L., and Racine R.
A measurement of isoplanatism with the high-resolution camera at the Canada-France-Hawaii telescope
Pub Astr.Soc. Pac. 103, 570-576, 1991.

[57]† Von der Lühe O.
Measurements of characteristics of image motion with a solar image stabilizing device
Astron. Astrophys. 205, 354-360, 1988.

[58]† Tatarskii V.I.
Wave Propagation in a Turbulent Medium
McGraw-Hill, New York, 1961.

[59]† Babcock W.
The possibility of compensating astronomical seeing
Publ. Astron. Soc. Pac. 65, 229–236, 1953.

[60]† Lillard R.L. and Schell J.D.
High-performance deformable mirror for wavefront correction
Proc. SPIE 2201, 740-753, 1994.

[61]† Kokorowski S.A.
Analysis of adaptive optical elements made from piezoelectric bimorphs
J.Opt.Soc.Am. 69, 181-187, 1979.

[62]† Vdovin G., Middelhoek, Bartek M., Sarro P. M., and Solomatine D.
Technology characterization and applications of adaptive mirrors fabricated with IC-compatible micromachining
Proc. SPIE 2534, 116- 120, 1995.

[63]† Gardner C.S., Welsh B.M., and Thompson L.A.
Design and performance analysis of adaptive optical telescopes using laser guide stars
Proc. IEEE 78,1721-1743,1990.

[64]† Happer W., MacDonald G.J., Max C.E., and Dyson F.J.
Atmospheric turbulence compensation by resonant optical backscattering from the sodium layer in the upper atmosphere
J. Opt. Soc. Am. A 11, 263-276, 1994.

[65]† Merkle F.
Adaptive Optics development at ESO
Proc.ESO Conf “Very Large Telescopes and their Instrumentation”, 639-656, 1998.

لاصة

هذا البحث بناء برنامج لإقتفاء اثر الأشعة البصرية خلال الأنظمة البصرية. يتـضمن هذا ال نامج:

١. اقتفاء اثر الأشعة البصرية العامة (**skew ray tracing**) خلال السطوح الكروية (**spherical surfaces**).
٢. اقتفاء اثر الأشعة البصرية العامة خلال السطوح ا خروطية أو ا سماة بالكارتيزية (**conic or Cartesian**).

لقد ت دراسة تأث عامل اللاتكور (ε) على معلمات (**parameters**)ا قراب العـاكس (**reflecting telescope**) ، قيد ث هذه الرسالة، بأستخدام شفرة أقتفـاء ألأشـعة البـصرية. ومعلمات التلسكوب هذه : هي قيم Δ (قيم ابتعاد السطح عن مستوي x-y ا ماس) ، و زيـوغ الأشعة البصرية الطولية (**LA**) وا ستعرضة (**TA**)، و الزاوية ال يصنعها الشعاع الساقط مع ا تجه العمود على السطح العاكس (ا رآة).

لقد كانت هذه الدراسة مفيدة لتصميم مقراب عاكس ذو مرآت ؛ حيث أعطـت هـذه الدراسة منظارا مناسبا لفهم أبعاد ا شكلة كما وأعطت رؤية لتقليل، وبشكل مباشـر، زيـوغ الأشعة البصرية وبالتا س أدآء النظام البصري.

أ از هذه الدراسة تطلب إعتماد حزمة أشعة بصرية موازية اما للمحور البصري، لذلك فان التصميم الناتج للنظام البصري سيكون مصححاً من الزيغ الكروي (**spherical aberration**) فقط.

لقد وظفت شفرة إقتفاء أثر الأشعة البصرية لأظهار أدآء السطوح العاكسة (ا رايا) عنـد تغي قيم عامل الاتكور (ε). كما و إعتماد زيوغ ألأشعة البصرية الطولية (LA) وا ـستعرضة (**TA**) كمقياس لأظهار أدآء أي من السطوح ا خروطية العاكسة أمام ε .

إن تقليل زيوغ أشعة الضوء قد من خلال تغي ،أولا، قيم نصف قطر تقـوس ا ـرآة الثانوية، وثانيا، من خلال تغي قيم ε بأستخدام مبدأ نظرية القيمة النهائية (النهاية العظمى والنهاية الصغرى).

إن التصميم النهائي للمقراب، ا نجز على اساس الدراسة، هو مقراب ذو مرآت طولـه البؤري **2.5m** وقطر مرآته ألأولية هو **1m**؛ ا رآة الأولية ذات قطع مكا ء و الثانوية ذات قطـع ناقص، وعامل اللاتكور للثانوية **ε=-0.21**.

ان الطول ا وجي ا عتمد حسابات ا اصة بالتلسكوب هو 550nm لأنه ثل منتصف الطيف ا رئي للضوء .

هوريةالعراق
وزارة التعليم العا والبحث العلمي
جامعة النهرين

دراسة حسابية ـ ليلة علمات ا قراب العاكس

أطروحة
مقدمة إ كلية العلوم جامعة النهرين وهي جزء من متطلبات نيل درجة
ماجستة علوم
الفيزياء

نور مد حسن ياس

(بكالوريوس علوم فيزياء ٢٠٠٤)

محرم ١٤٢٧ للهجرة
شباط ٢٠٠٧ للميلاد